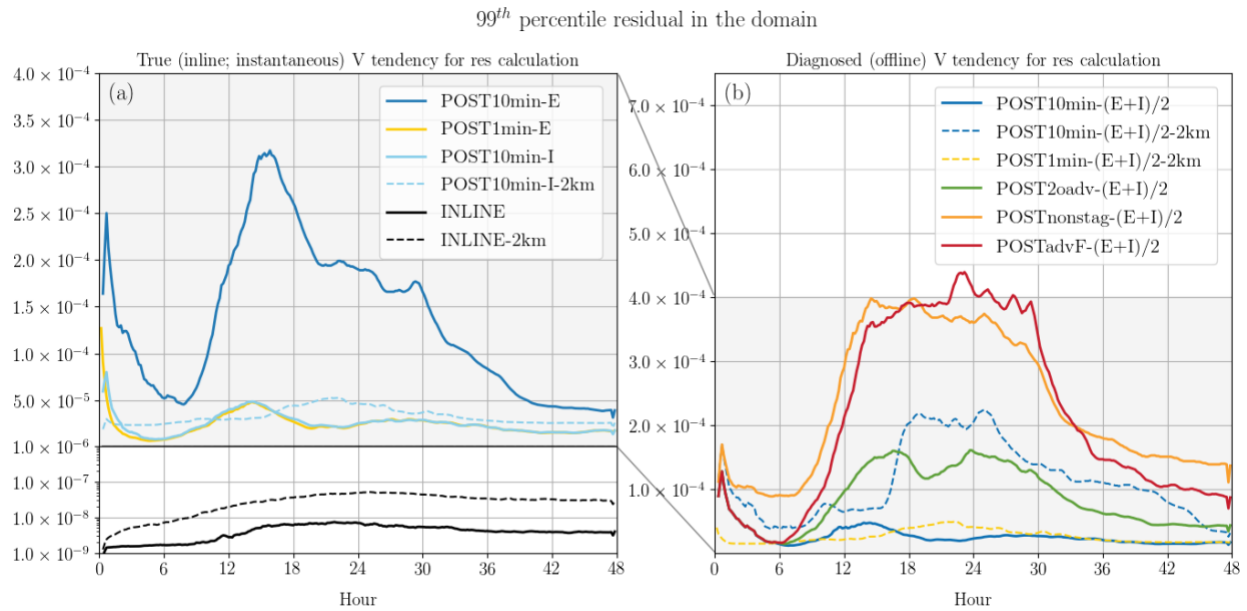


## Corrigendum

In the previous manuscript that was posted as a discussion paper in the scientific discussion forum of GMD, two figures contain incorrect information:

- (1) The original Figure 5 shows the maximum residual magnitude instead of the 99<sup>th</sup> percentile of the residual magnitude. The corrected Figure 5 appears below and it replaces the original Fig. 5 in the revised manuscript.



Corrected Figure 5. Evolution of the 99<sup>th</sup> percentile of the residual magnitude ( $ms^{-2}$ ) in the horizontal momentum V budget analysis. For the residual calculation, (a) uses the true V tendency (derived during the integration of the model) and (b) uses the post-diagnosed V tendency (Eq. (8)) as the lhs term. Different colors indicate different post-processed methods for estimating the rhs forcing terms. The residual obtained from the inline budget retrieval are in black. Solid and dashed lines are for the 10-km run and 2-km run, respectively.

- (2) The units noted next to the color bars in the original Figure 16 showing “( $ms^{-2}$ )” are incorrect. They have been corrected to “( $10^{-2} ms^{-2}$ )” in the revised manuscript.

The authors regret any confusion the above errors may have caused. Below we show our responses (marked in blue) to all referee comments (marked in black).

Referee #1 Patrick Hawbecker (hawbecke@ucar.edu)

Received and published: 5 November 2019

**General comments:** Towards the closure of momentum budget analyses in the WRF (v3.8.1) model by Chen et al. provides a clear and useful overview of the most common ways to obtain the various budget components from model output. While no novel techniques for calculating the budget components are developed within this study, the utility is within the comparison of existing techniques and highlighting the advantages and shortcomings of these techniques. For a study such as this, the rudimentary 2-dimensional setup is justified as it pertains strictly to the techniques to calculate the budget components and not the physical processes within the simulations. The study focuses analysis on the 99th percentile of the residuals for each method as well as the spatial locations and magnitudes of the individual budget components and residuals at instances in time throughout the simulation. The authors are careful to draw conclusions that are within the scope of the provided analysis. Overall, the paper is easy to follow and understand, remains on topic, and provides useful guidelines to the community and suggested best practices for calculating budget components moving forward. Further, the explanations of the steps involved in order to repeat such a study appear thorough and the recommended technique for the calculation of budget components is provided via a GitHub repository. As the model utilized is open sourced, it could be beneficial to the community to have this code submitted to be included in a future release.

[We appreciate the reviewer's positive responses to our work.](#)

**Specific comments:** If I am understanding the analysis correctly, it appears that analysis of the residual is confined to analyzing the 99th percentile whereas the figures show both large positive and negative values of the residuals. Should the lower end of the distribution (i.e. the 1st percentile) also be considered here? Further, is there a reason that only the extreme ends of the distribution are considered? If there is no reason, have you performed any sensitivity to the percentile chosen? [During the process of replying to this comment, we noticed a mistake that the original Figure 5 shows the maximum residual magnitude instead of the 99th percentile of the residual magnitude. Figure 5 \(see the Figure 5 in the Corrigendum\) has now been corrected in the revised manuscript. Note that while the maximum residual shows larger fluctuations with time \(with larger magnitude in general\) as compared to the 99th percentile residual, the general evolutions and the relative](#)

magnitudes among different methods remain unchanged and thus do not affect our conclusions significantly. We should have clarified that the “99<sup>th</sup> percentile residual” that we intended to show was in terms of the absolute magnitude. Such a choice was made simply because we were interested not only in the distribution of errors but also the peak magnitude regardless of the sign (i.e., the worst-case situation). Considering the maximum magnitude can be easily misled by a single outlier, the 99<sup>th</sup> percentile was chosen. This issue has been clarified in the revised manuscript (Line 211-213 and Fig. 5 caption): *”To understand how the peak error evolves with time, and to avoid reaching misleading conclusions based on one or more outlying values, the evolution of the 99<sup>th</sup> percentile magnitude of the residual term is shown.”*

To fully address reviewer’s concern, we also calculated the 95<sup>th</sup> percentile residual, which also shows the higher tail of the error distribution. Note that while the relative distribution of some post-processed methods varies with overall smaller magnitudes than their 99<sup>th</sup> percentiles, our conclusion remains qualitatively similar and the inline retrieval still has the smallest residual. We decided not to include Fig. R1 in the revised manuscript for the sake of simplicity. But the consistent results using the 95<sup>th</sup> percentile and the maximum residual have been added in the revised manuscript (Line 402-406).

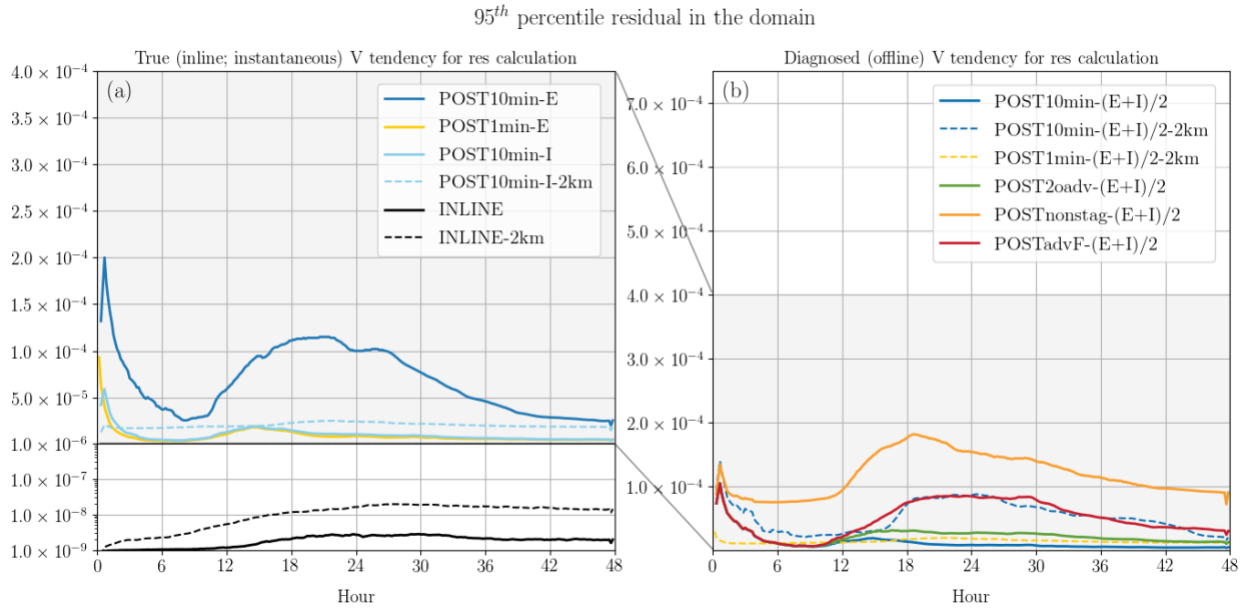


Figure R1. Same as the corrected Figure 5 but for the 95<sup>th</sup> percentile of the residual magnitude.

### Technical Corrections:

Figures 3 and 4 are somewhat difficult to see the “canceling out” between PGFBUOY and CUV in the filled contours, but the contour lines do help. Would a log-scaled colorbar be more appropriate here? Or maybe just adding panels to show the difference, PGFBUOY - CUV?

To address this issue, we have added a column showing the net force of PGF+COR for V and PGFBUOY+CUV for W to Figure 3 and Figure 4, respectively, in the revised manuscript.

Figure 4 caption: The second to last sentence explaining the rightmost column never mentions the the residual is contoured in the background and reads as though it is plotting strictly the acoustic-step components of PGFBUOY.

It was mentioned in the beginning of the caption: *“In each row, the shaded subplots from the left to right show the term of  $w$  tendency, advection (ADV), net vertical pressure gradient and buoyancy force (PGFBUOY), curvature (CUV) (white contours indicate the values exceeding the color bar) and residual”*. To make it clearer, we have modified the second to last sentence of the caption: *“The red (blue) contours shown in the rightmost column, laid on top of the residual (shading), indicate the small-step components of PGFBUOY with a positive (negative) value of...”*

Figure 5b legend: blue solid line “POST10imn” should be “POST10min”

Corrected. Thanks.

Line 313: “Moving the first term on the rhs of Eq. (17) is to the lhs...” should the word “is” be there?

The word is removed (Line 325 in the revised manuscript). Thanks for the correction.

Lines 318 smf 387: Section titled, “3.2.2 Results- horizontal momentum budget” and “3.2.3 Results- vertical momentum budget” should have a space between “Results” and the hyphen

The titles have been modified to “3.2.2 Results of horizontal momentum budget” (Line 330) and “3.2.3 Results of vertical momentum budget” (Line 407 in the revised manuscript).

Line 356-358: “Next, we repeated POST10min-(E+I)/2 but applied to the output data that have been interpolated to the universal/un-staggered grid same as the one for the pressure variable (p-grid) (POSTnonstag-(E+I)/2).” I recommend this sentence to be revised. It is not very clear what is going on. Throughout paper and figures: Phrases like “v tendency” sometimes include a capital “v” and other times a lowercase “v” (eg. Figure 2 figure and caption are all lower case, Figure 3 has both lower case and capitalized “v”, Figure 5 figure and caption are all capitalized; Lines 207-210 use both lowercase and capital). This should be made consistent throughout the paper.

The sentence has been modified as follows: *“Next, we repeated  $POST_{10min-(E+I)/2}$  but the calculation is applied after all the variables have been interpolated to the universal/un-staggered grid (pressure grid) ( $POST_{nonstag-(E+I)/2}$ ).”* Furthermore, we have clarified and made consistent in the revised paper that, when the lhs tendency term in a coupled momentum budget equation is referred, a capital “V” or “W” is used while the lowercase “v” or “w” tendency indicates the uncoupled momentum calculation (for Fig. 2 only).

In the revised manuscript, some text is added to Line 173-174: *“Figure 2 shows the two-day evolution of the 99th percentiles of v and w (hereafter the lower case indicates that the calculation uses the uncoupled momentum field) and their tendencies.”* and in Line 197-198: *“(coupled momentum; hereafter the momentum tendency with capital V or W refers to the lhs term derived for the budget analysis).”*

Line 441: “two time larger” should be “two times larger”

This sentence has been deleted in the revised manuscript.

Anonymous Referee #2

Received and published: 13 December 2019

This paper analyzes methods for horizontal and vertical momentum budget estimation, and compares them to an inline budget retrieval method using the WRF model in a simulated 2-D slantwise convection case. The authors presented clear analysis that point out the shortcomings of using offline budget calculations, and make suggestions to improve the estimation accuracy. The guidance should be useful to the modeling community, and especially to the inexperienced. The paper is generally well written and well organized, and figures are clear. Here are some questions for the authors to consider.

We appreciate the reviewer's positive responses to our work.

1. Despite the difficulties to obtain a closed budget through an offline method, people are careful using that approach to address the issue at hand. In the example presented in this paper, the slantwise convection simulation, can you say something about how inaccurate budget calculation could impact your study, and possibly affect the scientific conclusion?

One easy-to-interpret example is  $\text{POSTadvF}-(E+I)/2$  as shown in Fig. 14. When such offline budget analysis is done, i.e., following the advective-form momentum equation, the contribution of the advection process to the  $V$  tendency is severely overestimated. If the residual is neglected or not shown, authors and/or readers may falsely consider the advection process to be the dominant term governing the evolution of the slantwise updraft. This point has been added in the revised manuscript (Line 388-390).

2. It's unfortunate it is concluded that the vertical momentum budget via offline method doesn't work. The discussion may need some work. It is unclear why the acoustic mode would impact the budget since one would expect the larger terms are the vertical PGF, the buoyancy as well as the advection? Supposedly, the acoustic modes are meteorologically insignificant, how do you explain it significantly impact momentum budget? Could it be the nature of vertical motion? It is certainly very variable, and are small scale features itself.

We realized that the term "acoustic modes" might be misleading as they include not only the sound waves but also partially the gravity waves (Klemp et al. 2007). In the appendix of Klemp et al. (2007), it is mentioned that gravity wave modes are formed due to the designated terms that are

required for sound-wave propagation and “*Consequently, in this vertical coordinate (i.e., terrain-following hydrostatic pressure coordinate), the terms governing the acoustic and gravity wave modes are intermingled to the extent that it does not appear feasible to evaluate any of the gravity wave terms on the large time steps, even if one desired to do so.*” In fact, the WRF documentation (Skamarock et al. 2008) specifically mentions that smaller time step is designed to accommodate acoustic and gravity-wave modes. Although the terms “acoustic time step” and “acoustic modes” sometimes misleadingly refer to the small time step in the WRF documentation (Skamarock et al. 2008), we have changed the term “acoustic modes” to “small-step modes” in the revised manuscript to avoid confusion. The above information has been added in the revised manuscript (Line 228-235).

Furthermore, the difficulty of closing the budget for the  $W$  equation offline is also related to the fact that the model-solved  $W$  equation is implicit with a forward-in-time averaging operator applied on the small-step modes (originally termed as “acoustic modes”):

$$\bar{a}^{\tau} = \frac{1 + \beta}{2} a^{\tau + \Delta\tau} + \frac{1 - \beta}{2} a^{\tau}$$

where  $\beta$  is a user-specified parameter. The  $W$  budget equation can be written as:

$$W^{\tau + \Delta\tau} - W^{\tau} = \underbrace{R_W^{t^*}}_{\text{large-step forcing}} + \underbrace{\bar{a}^{\tau}}_{\text{small-step modes}}$$

and  $\bar{a}^{\tau}$  contains information of the geopotential variables at the time  $\tau + \Delta\tau$  (forecast time), whose tendency solver is coupled with the  $W$  tendency equation (see Eqs. (3.11) and (3.12) in Skamarock et al. (2008)). These components are not feasible for an offline calculation. Part of the above discussion was already included in the original manuscript but has been made clearer in the section “3.2.3 Results of vertical momentum budget” in the revised manuscript (starting from Line 407).

We also agree that the budget closure for vertical velocity could be difficult by nature due to its rapid variation in small scales. A closer examination shows that the large-step forcing term, PGFBUOY, varies largely, sometimes with sign changes, from step to step during one integration of the RK3 scheme. This point has also been added in Line 424-430 in the revised manuscript.

3. This is a minor issue. Would map projection or map-scale factor contribute to the accuracy of momentum budget? I understand it is not relevant in your test case, but map-scale factor will come in in a real data simulation. Should people consider it when doing offline calculations?

As a matter of fact, our inline retrieval tool also considers the map projection as the retrieval is coded following the model solver, i.e., the governing equations with map factors included. Physical terms are retrieved when its corresponding subroutine is called. For idealized cases on a Cartesian coordinate, the expression/calculation for the retrieved physical terms remains unchanged but simply that the map factor is 1 during the calculation. Note that we did not alter the original solver but only added codes to retrieve the desired information. For people who wish to conduct an offline calculation for a real case study, the most accurate way would be to follow the original formulas that consider map factors (Skamarock et al.'s (2008) Eqs. (2.23)-(2.25)). This point has been added in the revised manuscript (Line 539-541).

4. Would you like to contribute the inline budget code to the WRF repository?

We appreciate reviewer's suggestion. We would be interested in contributing to the WRF repository although the process requires some more code testing (including software, case and feature testing). While we are confident that the current added code can be similarly applied to the most recently released version of WRF model (v4.1), additional implementing and testing are also required to ensure compatibility.

**Other minor points:**

Lines 166-167: Why do you need the vertical velocity damping option? Using a microphysics could impact momentum tendency through density variations, and would affect the pressure field too.

The vertical velocity damping (Rayleigh damping) is activated for numerical stability when and where the vertical motion approaches the limiting Courant number. Its activation has nothing to do with the purpose of closing the budget analysis. Instead, this shows that the non-physical processes that affect the momentum tendencies (despite small magnitude except over the upper layers) can be considered and outputted via the inline retrieval tool. We agree with your idea that the microphysics can indirectly impact the momentum tendencies. Such information is added in the revised manuscript (Line 165-168):

*“For simplicity, only the Thompson microphysics scheme (Thompson et al. 2008) is used among all the parameterization schemes and the vertical-velocity damping (Skamarock et al., 2008, chapter 4.5.1) is also activated. The former does not directly contribute to the momentum fields*

*(although it can affect the momentum field indirectly through density and pressure variations) and the latter, contained in  $P_W$  in Eqs. (2) and (6), affects only the  $W$  momentum budget.”*

Page 9, section 3.2.1(b): The discussion may need to be made simpler and clearer. I was lost. With C-staggering, the computation of PGF for  $V$  is easy because pressure is naturally located at  $1/2DX$  to the north and south of  $V$  grid.

The section 3.2.1 is rewritten as follows:

*“...For example, the  $y$ -derivative of variable  $\Phi$  is calculated using the discrete operator:*

$$\frac{\partial \Phi}{\partial y}_{i,j,k} = \frac{1}{\Delta y} \left( \Phi_{i,j+\frac{1}{2},k} - \Phi_{i,j-\frac{1}{2},k} \right). \quad (9)$$

*The index  $(i,j,k)$  corresponds to a location with  $(x,y,\eta) = (i\Delta x, j\Delta y, k\Delta \eta)$ , where  $\Delta x, \Delta y$  and  $\Delta \eta$  are the grid lengths in the two horizontal and vertical directions (can be vertically stretched), respectively. The same expression applies for the  $x$ - or the  $\eta$ - derivatives. Grid staggering implies that different variables may be located on different grids, i.e., shifted by a half-grid point from the others as illustrated in Fig. 6. Depending on what variable the spatial derivatives are intended for, Eq. (9) should be carried out on the corresponding grid, which is not necessarily the same as the  $\Phi$  grid. For example, for the  $V$  tendency, all the associated forcing terms involving the spatial derivatives should be performed on the  $V$  grid. More specifically, to calculate the PGF term for the  $V$  tendency equation, the term  $\frac{\partial p}{\partial y}$  and the term  $\frac{\partial p}{\partial \eta}$  in Eq. (1) should be calculated on the  $V$  grid but not the pressure grid ( $p$  grid). Applying Eq. (9) for  $\frac{\partial p}{\partial y}$ , the  $V$  grid with location indices of  $(i, j - \frac{1}{2}, k)$  and  $(i, j + \frac{1}{2}, k)$  falls exactly on the  $p$  grid and hence no interpolation is required (red arrows in Fig. 6a). However, for  $\frac{\partial p}{\partial \eta}$ , the pressures on the  $V$  grid with indices of  $(i, j, k - \frac{1}{2})$  and  $(i, j, k + \frac{1}{2})$  must be obtained (red arrows in Fig. 6b) through linear interpolation using their surrounding closest four pressure values, e.g.,*

$$p_{V-grid(i,j,k-\frac{1}{2})} = \frac{\frac{1}{2}(p_{p-grid(i,j-1,k)} + p_{p-grid(i,j,k)}) \frac{\Delta \eta_{k-1}}{2} + \frac{1}{2}(p_{p-grid(i,j-1,k-1)} + p_{p-grid(i,j,k-1)}) \frac{\Delta \eta_k}{2}}{\frac{1}{2}(\Delta \eta_k + \Delta \eta_{k-1})} \quad (10)$$

*which is weighted by the irregular (stretched) vertical grid-lengths (Fig. 6b) ... ”*

Lines 384-385: What does this sentence mean?

The sentence has been modified as follows: *“Figure 5 also shows that any simplification that is inconsistent with the model solver can severely degrade the accuracy of the post-processed budget analysis.”* (Line 399-400 in the revised manuscript).

Section 3.2.3 Should vertical diffusion be considered in W budget? Would it account for some of the residual term in Fig 4?

No explicit diffusion is activated in our idealized setup. The implicit diffusion is embedded in the advection process (ADV in Fig. 4). However, the upper-level vertical velocity damping is activated and indeed considered when calculating the residual. This had been indicated in Line 211-213 in the original manuscript (Line 218-219 in the revised manuscript):

*“While the contribution from the upper-layer vertical velocity damping is not shown in Fig. 4 as it is generally small in the low layers, it is included as part of the rhs ( $P_W$ ) when calculating the residual for the inline budget analysis.”*

That said, the w damping is only important over the upper layers and thus not shown in Fig. 4 (also indicated in the figure caption).

Line 467: Disk space is another big issue.

Added (Line 494 in the revised manuscript). Thanks.

Ian Dragaud

iaandragaud@lamma.ufrj.br

Received and published: 13 December 2019

Dear authors, This paper is very interesting and helpful. I'm giving some suggestions for the paper, as follows:

Line 51: The paper explores and gives details about the computation of the individual terms from the model output and it is mentioned that an inline budget analysis has been reported only in a few studies. Then, it should be important to mention more details about these very few studies which have developed an inline budget analysis, especially the ones that used the WRF model. Did they get the terms directly from the model using the same procedures? The present work also used the same procedure as them?

We appreciate the reviewer's valuable suggestion. We agree that addressing the differences among our work and other inline-budget retrieval works is beneficial. We also appreciate you bringing our attention to other similar works. We have added Appendix A to the revised manuscript to address this issue as follows:

To our knowledge, there are at least three other similar inline budget retrieval works that have been done in the WRF model:

- *Lehner (2012) with WRF (v3.2.1)*
- *Moisseeva (2014), Moisseeva and Steyn (2014) with WRF (v3.4.1) – publicly available*
- *Potter et al. (2018) with WRF (v3.8.1) – publicly available*

- **Lehner (2012)** provides a very detailed instruction of how an inline budget retrieval is done for the WRF model, documented in the appendix of her thesis. The method/code was utilized in a published work studying the mechanisms of the thermally driven cross-basin circulation (Lehner and Whiteman 2014). However, the code was never made publicly available. From the document, it appears that Lehner (2012)'s general procedure of retrieving rhs budget terms during the model integration is essentially the same as our approach, which considers both the large-time-step and small/acoustic-time-step contributions. Furthermore, the individual contribution from different parametrization schemes that are activated in her study was also separately retrieved. While the

general method appears highly similar to our code, the momentum budget retrieval in Lehner (2012) only applies to the horizontal momentum (U and V) whereas our tool includes the budget retrieval for the vertical momentum (W) as well.

- **Moisseeva's (2014) and Moisseeva and Steyn's (2014)** inline budget retrieval tool is also for the horizontal momentum equations, U and V, only. Furthermore, it is simpler than Lehner (2012) as it does not include the acoustic/small-step correction terms. While the large-time-step, non-parameterized terms (e.g., pressure gradient terms, advection, Coriolis terms...) are individually retrieved, Moisseeva and Steyn (2014)'s Registry file only outputs one (summarized) term for all the parameterized physics. And if we understand their code correctly, a small error exists that the parametrized physics term is uncoupled with dry air density whereas the non-parameterized terms are coupled with dry air density.

- **Potter et al. (2018)**'s budget retrieval uses the code adapted from Moisseeva (2014), taking references from Lehner (2012), and is applied to the same version of the WRF model as used in this study (v3.8.1). More components are added from the version used in Moisseeva (2014), including the potential temperature budget, vertical velocity budget, the 6th order diffusion term, parametrized physics term decomposed to boundary and radiation schemes...etc. A major deviation between Potter et al. (2018)'s and our retrieval tools exists in that the acoustic/small-step components are still neglected in Potter et al. (2018). Since Potter et al. (2018) uses the same model version as in our study and their budget retrieval code is publicly available, we downloaded their code and compared the resulted budget analyses (both horizontal and vertical momentum) with ours. A WRF idealized test case of 2D squall line is applied (same case shown in Section 4 in our manuscript).

## V budget analysis

Utilizing our budget retrieval code:

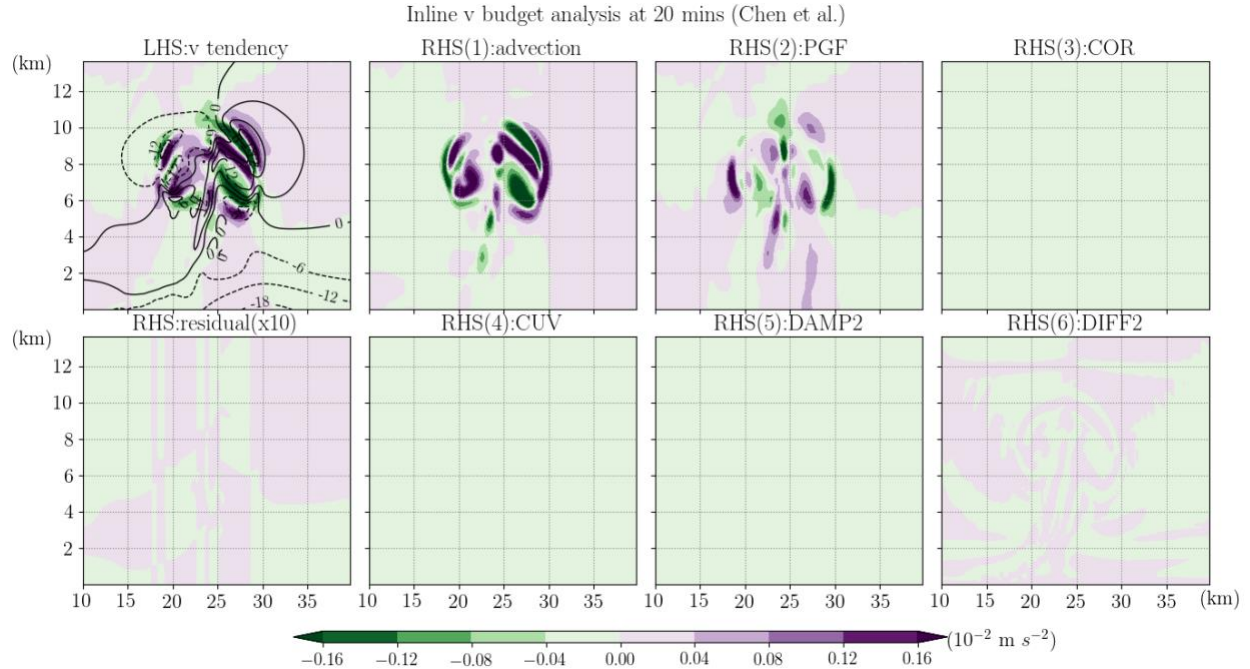


Figure R3-1. Our inline budget analysis of horizontal momentum,  $V$ , for the WRF ideal test case of 2-D squall line at 20 minutes of simulation time. Shading in subplots is indicated in the subtitle on the top, including the terms of  $V$  tendency, advection, horizontal pressure gradient force (PGF), Coriolis force (COR), curvature (CUV), damping (DAMP2), diffusion (DIFF2) and the residual (multiplied by 10 to emphasize its small magnitude as compared to the other terms). All terms are divided by  $\mu_d$  and thus have units of  $\text{ms}^{-2}$ . The black contours show the velocity,  $v$ , with an interval of  $6 \text{ ms}^{-1}$ .

Utilizing Potter et al. (2018)'s code: (note that a small bug was fixed for parallel computing)

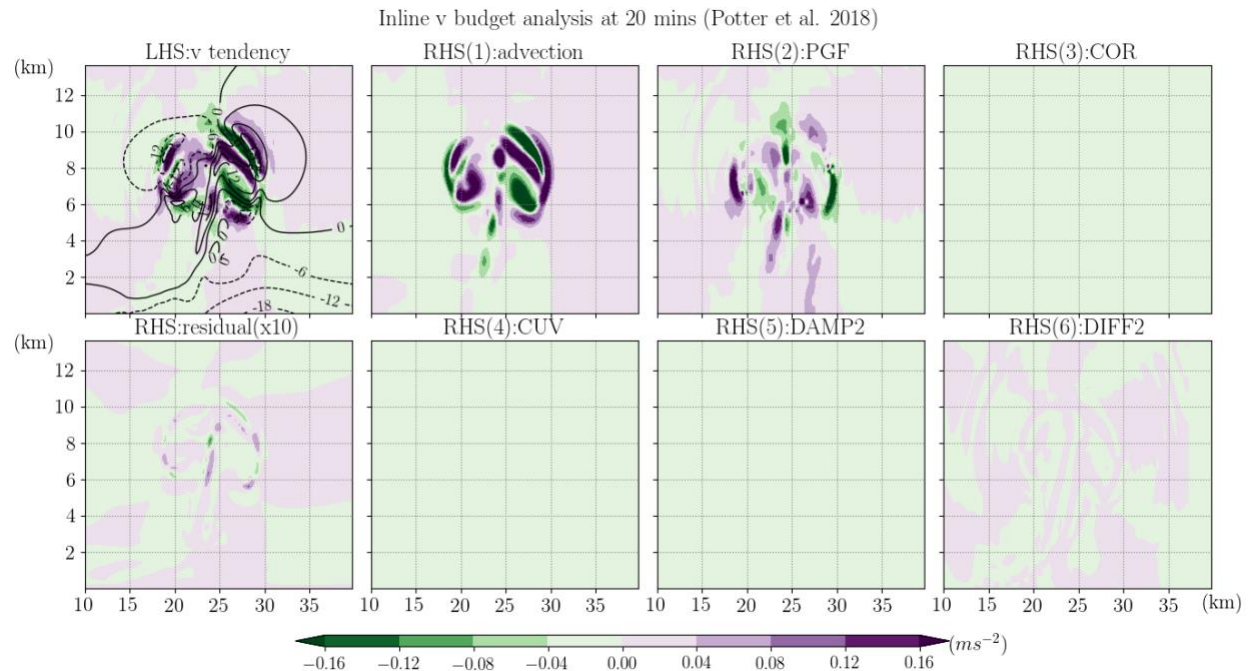


Figure R3-2. Same as Fig. R3-1 but utilizes the budget retrieval code from Potter et al. (2018).

It is no surprise to see the largest difference (yet the relative magnitude to the tendency term seems small) appears in the horizontal pressure gradient term (PGF), as this term contains information contributed by the acoustic/small-time-step integration.

## W budget analysis

Utilizing our budget retrieval code:

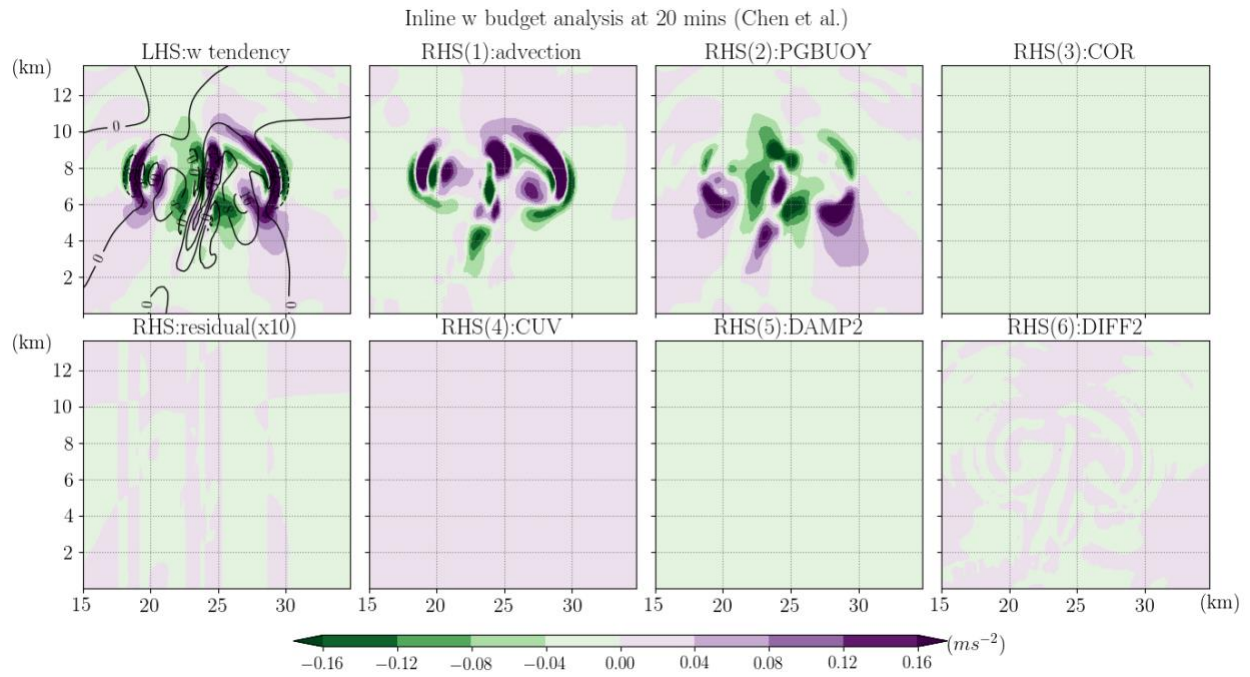


Figure R3-3. Same as Fig. R3-1 but for the W budget analysis.

Utilizing Potter et al. (2018)'s code: (note that a small bug was fixed for parallel computing)

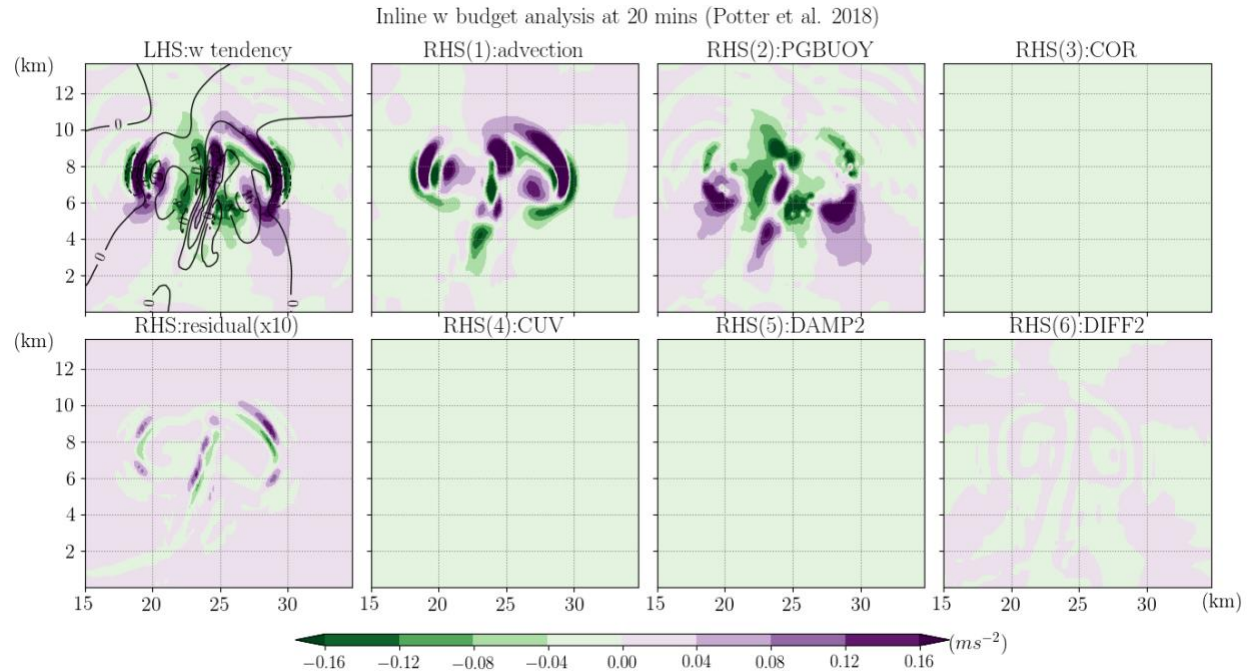


Figure R3-4. Same as Fig. R3-3 but utilizes the budget retrieval code from Potter et al. (2018).

The residual using Potter et al. (2018)'s tool appears larger for the W budget than that for the V budget. This is consistent with our result that the acoustic/small-step modes are more important in the W budget equation than in the V budget equation and thus ignoring them results in larger errors.

Nevertheless, it is a good sign that all the inline retrieval codes have high similarities in the general procedure even when different model versions are used among the above studies. Thus, we believe that one can easily apply the method described in this study to a newer WRF model version unless its dynamical core is fundamentally changed.

Line 52: Potter et al. (2018) also used an inline budget analysis in the paper "Dynamical Drivers of the Local Wind Regime in a Himalayan Valley" published in the Journal of Geophysical Research: Atmospheres, and it should be important to cite them. Their paper has also a supplement explaining the WRF code modifications and the modified files.

We appreciate the reviewer for providing this useful information. The paper has been cited in the modified manuscript and the discussion shown in the previous comment is added (Line 52, 577-589 in the revised manuscript).

Line 52: The Thesis of Moisseeva was cited in the paper, but she also published a paper "Dynamical analysis of sea-breeze hodograph rotation in Sardinia" in Atmospheric Chemistry and Physics journal. It is interesting to cite their article instead of the Thesis or to cite both. Their paper has also a supplement explaining the WRF code modifications and the modified files.

The published paper (Moisseeva and Steyn 2014) has also been added and discussed in our modified manuscript (Line 52 and Appendix A). Thanks.

**Line 193:** The authors added the inline calculation for the tendency term outside of the RK3 integration loop, after the microphysics scheme. However, as explained by Lehner (2012) and Moisseeva (2014), `ru_tend`, `rv_tend`, and `rw_tend` are the momentum tendency variables calculated by the WRF model and these variables can be outputted. So, as the tendency term is being calculated by the authors, it should be informed the advantages and reasons for doing it, in comparison to using the tendency variables calculated by the WRF model.

Thanks for bringing up this question, as this is a key point that should be clarified. The reason we added the calculation for U, V and W tendencies in the model is to calculate the "true" lhs terms in the budget equations, i.e., the simulated/observed changes of momentum fields with time. Because the purpose of the current study is to evaluate the balance/closure of the budget equations, the lhs term should be estimated independently from the retrieval of all the rhs terms. It is true that the momentum tendency terms, `ru_tend`, `rv_tend` ...etc, can be directly outputted from the WRF model by modifying the Registry file as done by Lehner (2012), Moisseeva (2014) and Potter et al. (2018). However, on checking the code, one would realize that these values are only the summation of all the large-time-step rhs forcing terms and do not necessarily represent the real momentum changes considering all the physics. For example, the microphysics, damping, acoustic/small-step modes, etc are not considered. Furthermore, because the `ru_tend`, `rv_tend`..etc are essentially the accumulation of all the large-time-step forcings after calling the subroutines for different physical processes (e.g., Coriolis force, advection...), there is no surprise that it would be equal to the summation of all the extracted large-time-step terms (with truncation errors and machine-rounding errors only). But one should note that these model-outputted tendency terms, `ru_tend`, `rv_tend`, etc, might deviate from the actual changes in the simulated momentum fields.

The above discussion has been added in Line 198-202 and Line 589-592 in the revised manuscript.

Line 523: Although the authors made available the adapted WRF v3.8.1, it is important to mention which files were modified. It is very helpful to know it since some researchers can compare the default files with the modified files and apply the modifications in other versions of the model, or just to understand in details which modifications were done.

We appreciate reviewer's suggestion. The full code of the adapted WRF v3.8.1 on our GitHub repository has tags for the fortran files that have been changed from the defaults. But we agree that it would be beneficial to explicitly write out the changed files in the paper. This information has been added in our modified manuscript (see Line 552-556):

*"In this repository, all the files that remain unchanged from the defaults are tagged as "Initial commit". The modified files for the budget retrieval include the Registry.EM\_COMMON within the directory Registry; module\_diag\_misc.F, module\_diagnostic\_driver.F and module\_physics\_addtendc.F within the directory phys; module\_after\_all\_rk\_steps.F, module\_big\_step\_utilities\_em.F, module\_em.F, module\_first\_rk\_step\_par2.F, module\_small\_step\_em.F and solve\_em.F within the directory dyn\_em."*

# Towards the closure of momentum budget analyses in the WRF (v3.8.1) model

Ting-Chen Chen, Man-Kong Yau and Daniel J. Kirshbaum  
Atmospheric and Oceanic Sciences Department, McGill University, Montreal, H3A0B9, Canada

5 Correspondence to: Ting-Chen Chen (ting-chen.chen@mail.mcgill.ca)

**Abstract.** Budget analysis of a tendency equation is widely utilized in numerical studies to quantify different physical processes in a simulated system. While such analysis is often post-processed when the output is made available, it is well acknowledged that the closure of a budget is difficult to achieve without temporal and/or spatial averaging. Nevertheless, the development of errors in such calculations has not been systematically investigated. In this study, an inline budget retrieval method is first developed in the WRF v3.8.1 model and tested on a 2D idealized slantwise convection case with a focus on the momentum equations. This method extracts all the budget terms following the model solver, which gives a high accuracy with a residual term always less than 0.1% of the tendency term. Then, taking the inline values as truth, several offline budget analyses with different commonly-used simplifications are performed to investigate how they may affect the accuracy of the estimation of individual terms and the resultant residual. These assumptions include using a lower-order advection operator than the one used in the model, neglecting grid staggering, or following a mathematically equivalent but transformed format of the governing equations. Errors in these post-processed analyses are found mostly over the area where the dynamics are the most active, thus impairing the subsequent physical interpretation. A maximum 99<sup>th</sup> percentile residual can reach ≥50% of the concurrent tendency term, indicating the danger of neglecting the residual term as done in many budget studies. This work provides general guidance not only for budget diagnoses with the WRF model but also for minimizing the errors in post-processed budget calculations.

## 1 Introduction

The atmosphere is a complex system with different scales of motion. Its dynamics are governed by a set of fluid equations based on the fundamental laws of physics. Although the equation set cannot be solved analytically, numerical models can be used to simulate the observed weather and climate systems to improve our understanding of the atmosphere. Due to the complexity and nonlinearity of the numerical models, budget analysis is often employed to interpret the results by quantifying the contribution of each term (i.e., physical process) in a tendency equation that governs the evolution of a certain quantity in the simulated system. The accuracy of a given budget analysis can be estimated from the residual term, defined as the difference between the tendency term on the left-hand side (lhs) of the equation and the summation of all the forcing terms on its right-hand side (rhs). Budget analysis has been performed on diverse properties (e.g., momentum, temperature, water vapor,

Deleted: -
Deleted: potential rise
Deleted: the
Deleted: calculation
Deleted: 02
Deleted: post-processing
Deleted:
Deleted: the C
Deleted: grids
Deleted: -
Deleted: equation
Deleted: 800
Deleted: applying an inline
Deleted: retrieval to
Deleted: processing

45 vorticity, etc) of many systems on various scales, including the Madden-Julian oscillation (MJO; e.g., Kiranmayi and Maloney, 2011; Andersen and Kuang, 2012), tropical cyclones (e.g., Zhang et al., 2000; Rios-Berrios et al., 2016; Huang et al., 2018), squall lines (e.g., Sanders and Emanuel, 1977; Gallus and Johnson, 1991; Trier et al., 1998), supercell thunderstorms (e.g., Lily and Jewett, 1990) and so on.

50 Despite the popularity of the budget analysis, it is generally acknowledged that, in model post-processing analysis, obtaining a closed budget with a negligible residual is difficult (e.g., Kanamitsu and Saha, 1996) and has been accomplished mostly in time- or domain-averaged budget calculations (e.g., Lilly and Jewett, 1990; Balasubram and Yau, 1994; Arnault et al., 2016; Kirshbaum et al., 2018; Duran and Molinari, 2019). Even in the case of averaged budgets, the residual term that contains non-explicitly-diagnosed physics can be larger than the tendency term (e.g., Liu et al., 2016) and many studies simply do not display the residual, making the proper interpretation of the budget analysis difficult.

55 The “residual analysis method” is sometimes utilized to obtain an indirect estimation of the physical processes that are hard to diagnose or are unresolved in a set of analysis/observational data. In such cases, a non-negligible residual is sometimes used to gain insight into such processes. However, as just discussed, the residual term also contains the inaccuracies associated with the calculations within the budget analysis (e.g., Kornegay and Vincent, 1976; Abarca and Montgomery, 2013). It is thus unclear whether the unresolved physics in such data sets indeed comprise of the main component of the residual without considering the contributions of other sources of errors in the budget calculation (Kuo and Anthes, 1984). Whereas it is almost impossible to separate the subgrid-scale, unresolved processes from other errors in reanalysis or observational data (e.g., Hodur and Fein, 1977; Lee 1984), the focus of this study is on numerical model data where the local tendency and all the associated resolved and parameterized physics can be obtained from the model. Thus, the residual term in this study specifically refers to errors in the budget calculation.

65 To reduce the residual, an inline budget analysis that extracts all the terms of a prognostic equation directly from the model during its integration is generally the most accurate. However, the procedure has been reported only in a few studies (e.g., Zhang et al., 2000; Lehner, 2012; Moiseeva, 2014; Moiseeva and Steyn, 2014; Potter et al., 2018; see Appendix A for a summary and comparison among these works). Most other studies still conduct the offline/post-processing budget analysis when the output is made available after the model integration. Some specific suggestions have been given in the past regarding how to reduce the error of post-processed budget analysis. For example, Lilly and Jewett (1990) emphasized the importance of evaluating terms using the same differencing scheme, grid stretching, and grid staggering as that used in the simulation model. However, it is uncertain whether these rules have been widely followed, and how much of a reduction in residual can be obtained with this approach.

75 In some post-processed budget analyses, transformed equations with different assumptions from those in the model are used and naturally lead to errors in the budget results. On the other hand, even when the same form of the equations is followed, errors can still arise from multiple sources during the post-processing. Some errors are inherent in the time discretization scheme of the model, some are traced to the numerical methods in solving the temporal/spatial derivatives with finite differencing (e.g., Kuo and Anthes, 1984), and others might emerge during the inter/extrapolation from model grids to analysis

Deleted:

Deleted: unsolved

Deleted: contribution

Deleted: unsolved

Deleted: ).

Deleted: processing

85 grids (e.g., Lilly and Jewett, 1990). While the tendency term is often the result of a few cancellations among competing forcing terms, the seemingly non-dominant terms may be as important as the large forcing terms in determining the sign and the value of the tendency. Thus, an incorrect estimation of even a small term may result in a residual with magnitude comparable to the tendency term, thus hindering the subsequent physical interpretation.

A few models, such as Cloud Model 1 (CM1; Bryan and Fritsch, 2002) and High Resolution Limited Area Model (HIRLAM; Undén et al., 2002), include inline budget diagnoses that users can choose to include in the model output. However, many other commonly used models (e.g., Fifth-Generation NCAR / Penn State Mesoscale Model (MM5; Grell et al., 1994), Weather Research and Forecasting Model (WRF; Skamarock et al., 2008), the Advanced Regional Prediction System (ARPS; Xue et al., 2000, 2001) and the Regional Atmospheric Modeling System (RAMS; Pielke et al., 1992)) do not have this capability. In this study, we develop an inline momentum budget retrieval tool in the Advanced Research WRF model, one of the most widely-used numerical weather prediction models. During the period 2011-15, there were on average 510 peer-reviewed journal publications involving WRF per year (Powers et al., 2017). Given the widespread use of WRF for both real-case and idealized modelling, such a budget tool may prove useful in numerous applications. In our budget diagnosis, each contributing term is extracted during the model integration and stored as a standard output. In so doing, we essentially solve the prognostic variables as done in the model so that the two sides of the tendency equation are always in balance regardless of the output time interval. By taking the results from the inline budget analysis as truth, we then perform several different post-processing budget analyses with commonly-made simplifications or a different format of equation. Comparisons between the post-processed budgets and the inline/true values are made to investigate the potentially large errors in each forcing term and the resultant residuals.

## 2 Model and numerical setup

### 105 2.1 Model and momentum equations

The WRF configuration used in this study is a two-dimensional [(y, z); no variation in the x direction], fully compressible, non-hydrostatic and idealized version of the Advanced Research WRF model, version 3.8.1 (Skamarock et al., 2008). Here we briefly revisit the parts that are relevant to the momentum budget analysis. The governing equations in the WRF model are cast on a terrain-following dry-hydrostatic pressure coordinate. This vertical coordinate,  $\eta$ , is defined as

$$110 \quad \eta = (p_{dh} - p_{dh\_top})/\mu_d$$

where  $p_{dh}$  is the hydrostatic pressure of the dry air and  $\mu_d$  represents the mass of the dry air per unit area in the column,  $\mu_d = p_{dh\_sfc} - p_{dh\_top}$  where  $p_{dh\_sfc}$  and  $p_{dh\_top}$  indicate the values of  $p_{dh}$  at the surface and the top of the dry atmosphere, respectively.

To ensure conservation properties, the model equations are formulated in flux form, with the prognostic variables coupled with  $\mu_d$ . The flux-form momentum components are defined as

- Deleted: offer
- Deleted: the choice
- Deleted: namelist file to
- Deleted: the budget terms for prognostic variables.
- Deleted: the
- Deleted: to write out all these terms into the standard history output files.
- Deleted: method
- Deleted: are
- Deleted: the method
- Deleted: and
- Deleted: processing
- Deleted: potential increase in

$$U = \mu_d u, \quad V = \mu_d v, \quad W = \mu_d w, \quad \Omega = \mu_d \frac{d\eta}{dt}.$$

where  $u, v$  and  $w$  are the zonal, meridional and vertical velocities, respectively. Note that the dry-mass-coupled velocities ( $U, V, W$ ) on coordinates  $(x, y, z)$  have units of  $\text{Pa m s}^{-1}$ , and the dry-mass-coupled vertical velocity on  $\eta$  coordinate,  $\Omega$ , has a unit of  $\text{Pa s}^{-1}$ . For the idealized 2D case on a  $f$ -plane as in this study, the momentum equations in the WRF model are written as

$$\underbrace{\frac{\partial V}{\partial t}}_{\text{V tendency}} = \underbrace{-\nabla \cdot (\vec{V}V)}_{\text{advection ADV}} + \underbrace{-\mu_d \alpha \frac{\partial p}{\partial y} - \frac{\alpha}{\alpha_d} \frac{\partial p}{\partial \eta} \frac{\partial \phi}{\partial y}}_{\text{horizontal pressure gradient force PGF}} + \underbrace{-fU}_{\text{Coriolis COR}} - \underbrace{\left(\frac{vW}{r_e}\right)}_{\text{curvature CUV}} + \underbrace{P_V}_{\text{remaining (parameterized) physics}} + res \quad (1)$$

$$\underbrace{\frac{\partial W}{\partial t}}_{\text{W tendency}} = \underbrace{-\nabla \cdot (\vec{V}W)}_{\text{advection ADV}} + \underbrace{g \left( \frac{\alpha}{\alpha_d} \frac{\partial p}{\partial \eta} - \mu_d \right)}_{\text{net vertical pressure gradient and buoyancy force PGFBUOY}} + \underbrace{\left( \frac{uU + vV}{r_e} \right)}_{\text{curvature CUV}} + \underbrace{P_W}_{\text{remaining (parameterized) physics}} + res \quad (2)$$

where

$$-\nabla \cdot (\vec{V}a) = -\frac{\partial(Ua)}{\partial x} - \frac{\partial(Va)}{\partial y} - \frac{\partial(\Omega a)}{\partial \eta} \quad (3)$$

is the flux-form advection,  $p$  is the full pressure with inclusion of vapor,  $\phi$  is the geopotential,  $f$  is the Coriolis parameter,  $r_e$  is the mean earth radius, and  $\alpha$  and  $\alpha_d$  are the full and dry-air specific volume, respectively. In our selected microphysics scheme (Thompson et al., 2008), six hydrometeors are included, and thus  $\alpha = \alpha_d (1 + q_v + q_c + q_r + q_i + q_s + q_g)^{-1}$ , where

$q_v, q_c, q_r, q_i, q_s$  and  $q_g$  are the mixing ratios for water vapor, cloud, rain, ice, snow, and graupel, respectively. The rhs forcing terms for the V tendency include the flux-form advection (ADV), horizontal pressure gradient force (PGF), Coriolis force (COR), vertical (earth-surface) curvature (CUV) and the remaining physics ( $P_V$ ). For the W tendency, the rhs forcings contain the flux-form advection (ADV), net force between the vertical pressure gradient and buoyancy (PGFBUOY), curvature effect (CUV) and the remaining physics ( $P_W$ ). The remaining physics may include diffusion, vertical velocity damping processes and other parameterized physics, depending on the model setup. Note that for closing the budget analysis, all the known physics processes that come into play should be explicitly written in the equation and be diagnosed or directly retrieved from the model. The residual ( $res$ ) is added on the last rhs term of Eqs. (1) and (2) to represent the imbalance between the two sides of the equation during budget analysis, but it is not part of the original equations solved in the model.

To develop an inline budget retrieval tool, it is very important to understand how these prognostic variables are advanced in the WRF model. Governing equations are first recast to perturbation forms with respect to a dry hydrostatically-balanced reference state that is strictly a function of height only (defined at initialization) to reduce truncation errors and machine rounding errors. Specifically, variables of  $p, \phi, \alpha_d$  and  $\mu_d$  are separated into reference and perturbation components, e.g.,  $p(x, y, \eta, t) = \bar{p}(z) + p'(x, y, \eta, t)$ . The introduction of these perturbation variables only changes the expressions for rhs terms PGF and PGFBUOY in Eqs. (1) and (2), which will not be shown here for simplicity. Readers can refer to Skamarock et al. (2008, chapter 2.5) for more details.

Adapting from Skamarock et al. (2008), Figure 1 summarizes the WRF integration strategy. The integration is wrapped by a third-order Runge-Kutta (RK3) scheme, in which the prognostic variables (generalized as  $\Phi$  here) are advanced from  $t$  to  $t + \Delta t$  given their corresponding partial differential equations,  $\frac{\partial \Phi}{\partial t} = F(\Phi)$ , following a three-step strategy:

$$\begin{aligned}\Phi^* &= \Phi^t + \frac{\Delta t}{3} F(\Phi^t) \\ \Phi^{**} &= \Phi^t + \frac{\Delta t}{2} F(\Phi^*) \\ \Phi^{t+\Delta t} &= \Phi^t + \Delta t F(\Phi^{**})\end{aligned}\quad (4)$$

where  $\Delta t$  is the model integration time step and  $F$ , defined as the large-step forcing, represents the summation of all the rhs terms of Eqs. (1) and (2) excluding the residual. Although the parameterized forcings stay fixed from step one to three as most of the parameterization schemes are called only once at the first RK3 step, the rest of the non-parametrized forcings and thus the total  $F$  are changed with the updated  $\Phi^*$  and  $\Phi^{**}$  at the second and third RK3 step. Within each RK3 step, a subset of time integration with a relatively smaller time step is embedded to accommodate high-frequency modes for numerical stability (Wicker and Skamarock, 2002; Klemp et al., 2007; Skamarock et al., 2008). A maximum number of small steps in one model integration step can be specified by the user. To improve accuracy in the temporal solver, the variables being advanced in this small-step integration are the temporal perturbation fields, defined by the deviation from their more recent RK3 predictors:

$\Phi'' = \Phi - \Phi^{t*}$ , where  $\Phi^{t*} = \Phi^t, \Phi^*$  and  $\Phi^{**}$  for the first, second, and third RK3 step, respectively. Thus, the perturbation momentum equations to be solved are driven by the large-step forcings and the small-step (sometimes referred as “acoustic-step” (e.g., Skamarock et al. 2008)) corrections:

$$\frac{\partial V''}{\partial t} = \left[ \underbrace{-\nabla \cdot (\vec{V}V)}_{\text{advection ADV}} \underbrace{-\mu_d \alpha \frac{\partial p}{\partial y} - \frac{\alpha}{\alpha_d} \frac{\partial p}{\partial \eta} \frac{\partial \phi}{\partial y}}_{\text{horizontal pressure gradient force PGF}} \underbrace{-fU}_{\text{Coriolis COR}} \underbrace{-\left(\frac{vW}{r_e}\right)}_{\text{curvature CUV}} + \underbrace{P_V}_{\text{remaining (parameterized) physics}} \right]^{t*}$$

large-step forcings (F)

$$-\frac{\alpha^{t*}}{\alpha_d^{t*}} \left[ \mu_d^{t*} \left( \alpha_d^{t*} \frac{\partial p''}{\partial y} + \alpha_d^{t*} \frac{\partial p}{\partial \eta} \frac{\partial \phi''}{\partial y} \right) + \frac{\partial \phi^{t*}}{\partial y} \left( \frac{\partial p''}{\partial \eta} - \mu_d^{t*} \right) \right]$$

small-step modes (ACOUS)

$$\frac{\partial W''}{\partial t} = \left[ \underbrace{-\nabla \cdot (\vec{V}W)}_{\text{advection ADV}} + \underbrace{g \left( \frac{\alpha}{\alpha_d} \frac{\partial p}{\partial \eta} - \mu_d \right)}_{\text{net vertical pressure gradient and buoyancy force PGFBUOY}} + \underbrace{\left( \frac{uU + vV}{r_e} \right)}_{\text{curvature CUV}} + \underbrace{P_W}_{\text{remaining (parameterized) physics}} \right]^{t*}$$

large-step forcings (F)

Deleted: time derivative

Deleted: /acoustic

Deleted: for acoustic

Deleted: users

Deleted: acoustic

Deleted:  $-\frac{\alpha^{t*}}{\alpha_d^{t*}} \left[ \mu_d^{t*} \left( \alpha_d^{t*} \frac{\partial p''}{\partial y} + \alpha_d^{t*} \frac{\partial p}{\partial \eta} \frac{\partial \phi''}{\partial y} \right) + \frac{\partial \phi^{t*}}{\partial y} \left( \frac{\partial p''}{\partial \eta} - \mu_d^{t*} \right) \right]$   
acoustic-step modes (ACOUS)

$$+g \left( \left( \frac{\alpha^{\tau^*}}{\alpha_d^{\tau^*}} \right) \left[ \frac{\partial}{\partial \eta} \left( C \frac{\partial \phi''}{\partial \eta} \right) + \frac{\partial}{\partial \eta} \left( \frac{c_s^2}{\alpha^{\tau^*}} \frac{\partial \theta''}{\partial \eta} \right) \right] - \mu_d'' \right) \quad (6)$$

small-step modes (ACOUS)

185 where  $\tau$  indicates the time in the small-step integration, and  $C$  as well as  $c_s^2$  are sound-wave related terms (Skamarock et al., 2008, chapter 3.1.2). Here we leave out the details regarding the small-step terms that are irrelevant to the inline budget retrieval. Note that the overbar in Eq. (6) indicates a forward-in-time averaging operator for the small-step modes to damp instabilities associated with vertically-propagating sound waves (see Eq. (3.19) in Skamarock et al., 2008). Equations (5) and (6) are the ones used to integrate the prognostic momentum fields in the WRF model. For each RK3 step, after the total large-

190 step forcing  $F$  is determined,  $V''$  and  $W''$  are defined and advanced within the small-step scheme by a loop that adds  $F$  multiplied by a time interval,  $\Delta\tau$ , (varies with different RK3 steps; see Fig. 1) and the small-step forcing (ACOUS). After the small-step integration loop ends,  $V$  and  $W$  are then recovered from their temporal perturbation fields and moved forward to the next RK3 step. While it is not relevant to the momentum equations discussed here, for some variables directly contributed by the microphysics scheme, the associated contribution should be considered after the RK3 integration loop ends as the

195 microphysics are integrated externally using an additive time splitting (Fig.1) (Skamarock et al., 2008, chapter 3.1.4).

## 2.2 Experimental setup

The main discussion of this study will focus on a 2D ( $y, z$ ) idealized simulation of slantwise convection. This process releases conditional symmetric instability (CSI), which can be idealized by assuming no flow variations along the direction of thermal winds (denoted as the  $x$  direction in our setup; Markowski and Richardson, 2010, chapter 3.4). The initial field consists of a thermally-balanced uniform westerly wind shear in  $x$ . This baroclinic environment contains no conditional (gravitational) instability, no inertial stability, and no dry symmetric instability, but does contain some CSI. A two-dimensional bubble containing perturbations of potential temperature and zonal wind is added to initiate convection and a slanted secondary circulation ( $v, w$ ). See Appendix B for more details about the experimental setup. The domain size is 1600 km and 16 km in the  $y$  and  $z$  direction, respectively, with a horizontal grid length of 10 km and 128 vertical layers. The model integration time

205 step is 1 minute. For simplicity, only the Thompson microphysics scheme (Thompson et al. 2008) is used among all the parameterization schemes and the vertical-velocity damping (Skamarock et al., 2008, chapter 4.5.1) is also activated. The former does not directly contribute to the momentum fields (although it can affect the momentum field indirectly through density and pressure variations) and the latter, contained in  $P_W$  in Eqs. (2) and (6), affects only the  $W$  momentum budget. The WRF model offers different orders of advection operators, and the default third- and fifth-order operators are selected for the

210 vertical and horizontal in this case, respectively. Most of the subsequent analyses and discussion are based on this slantwise convection case with a 10-km grid length unless specified otherwise. Two other simulations, one of which uses the same setup but with an increased horizontal resolution of 2 km, will be discussed in Section 4.

Figure 2 shows the two-day evolution of the 99<sup>th</sup> percentiles of  $v$  and  $w$  (hereafter the lowercase indicates that the calculation uses the uncoupled momentum field) and their tendencies. For the 10-km case, the horizontal velocity reaches its

$$\text{Deleted: } +g \left( \left( \frac{\alpha^{\tau^*}}{\alpha_d^{\tau^*}} \right) \left[ \frac{\partial}{\partial \eta} \left( C \frac{\partial \phi''}{\partial \eta} \right) + \frac{\partial}{\partial \eta} \left( \frac{c_s^2}{\alpha^{\tau^*}} \frac{\partial \theta''}{\partial \eta} \right) \right] - \mu_d'' \right)$$

acoustic-step modes (ACOUS)

Deleted: acoustic

Deleted: acoustic

Deleted: trivial

Deleted: acoustic

Deleted: acoustic

Deleted: acoustic

Deleted: acoustic

Deleted: ) and assumes no variation

Deleted: inserted

Deleted: the appendix

Deleted: only affects the  $W$  momentum budget (

Deleted: ).

Deleted: advection

Deleted: in this paper

Deleted: Sect.

peak in about 20 hours, a few hours after the vertical velocity reaches its maximum, and then undergoes a weakening. Both v and w tendencies are maximized at around 15 hours. To understand the evolution of the associated flow dynamics, a momentum budget analysis serves as a natural choice. However, as a preliminary step prior to carrying out such analysis, we focus only on the technical discussion of the budget-analysis methodology. The physical interpretation of the motion is beyond the current scope and will be presented in a subsequent paper.

### 3 Methodology and results

#### 3.1 Inline momentum budget analysis

For the inline budget analysis, all the terms are retrieved directly from the model for all the integration time steps, and therefore they represent the “instantaneous” terms that act over the specified short integration time window. For the large-step forcing, the WRF model accumulates all forcing terms at the beginning of each RK3 step. To separate them, we simply take the difference before and after WRF calls the subroutine for each large-step forcing, store their values separately, and output only the values at the third RK3 step (the total forcing is  $F(\Phi^{**})\Delta t$  as shown in Fig. 1). As for the contribution of the small-step modes, they are obtained by accumulating over all the small steps in the third RK3 step ( $[ACOUS\ sum]$  shown in Fig. 1). It is worth noting that Eq. (6) is a vertically implicit equation that couples with the geopotential tendency equation (Skarmarock et al. 2008 and Klemp et al. 2007). A tri-diagonal equation for the vector W (involving three grid points in the vertical direction) is thus solved (Sato 2002). This means that W is not advanced by linear additions in the small-step/acoustic scheme. To ensure the closure of the inline retrieval budget, we simply take the total changes that are contributed by the implicit solver in the acoustic scheme as small-step modes of W in the third RK3 step. Note that this way does not violate the original W equation in Eq. (6). The contribution from these accumulated small-step modes in the V and W tendency budgets are combined with their large-step PGF and PGFBUOY, respectively, as they share the same mathematical expressions. Finally, we add the inline calculation for the tendency term outside of the RK3 integration loop, after the microphysics scheme:

$$\frac{\partial \Phi^{t+\Delta t}}{\partial t} \equiv \frac{\Phi^{t+\Delta t} - \Phi^t}{\Delta t} \quad (7)$$

where  $\Delta t$  is the model integration time step and  $\Phi$  represents V or W (coupled momentum; hereafter the momentum tendency with capital V or W refers to the lhs term derived for the budget analysis). The values of  $\Phi$  at times  $t$  and  $t + \Delta t$ , the latter denoted by superscripts, are termed the current and predicted states, respectively. Note that while variables of momentum tendencies (specifically named as “ru tend, rv tend and rw tend”) can be directly outputted from the WRF model by modifying the Registry file, these variables do not necessarily represent the actual momentum changes that consider all the physical (e.g., microphysics, small-step modes) and non-physical processes (e.g., damping) but only the summation of all the large-step forcings.

Figures 3 and 4 present the results of the inline budget analysis for horizontal momentum and vertical momentum, respectively, at three selected times (6, 12 and 16 h). To demonstrate the momentum changes in a common physical unit

Deleted: a

Deleted: companion

Deleted: acoustic

Deleted: acoustic

Deleted: grids

Deleted: insure

Deleted: acoustic

Deleted: acoustic

Deleted: .

Deleted: .

Deleted: instants of

Deleted: hours.

(velocities;  $\text{ms}^{-1}$ ), every term of the flux-form budget equation shown in this paper is divided by the dry-air mass,  $\mu_d^{t+\Delta t}$  (so that, for example, the V tendency has a unit of  $\text{ms}^{-2}$ ). The magnitude of the V tendency intensifies during this period with local maxima on the order of  $10^{-4}$  to  $10^{-3} \text{ ms}^{-2}$  (Fig. 3). Two forcing terms, PGF and COR, are a few times larger than the ADV term but generally offset each other, making the ADV term of comparable importance in determining the tendency. The CUV term for V tendency is generally small and thus not shown in Fig. 3. The residual, obtained from Eq. (1) with  $P_V$  equal to zero, is always smaller than  $10^{-7} \text{ ms}^{-2}$  during the entire two-day simulation (not shown). To understand how the peak error evolves with time, and to avoid reaching misleading conclusions based on one or more outlying values, the evolution of the 99<sup>th</sup> percentile magnitude of the residual term is shown. Figure 5 shows that it reaches a value of about  $7 \times 10^{-9} \text{ ms}^{-2}$  at around 15 hours. Recall that the 99<sup>th</sup> percentile magnitude of the simulated v tendency has a peak of  $7 \times 10^{-4} \text{ ms}^{-2}$  (Fig. 2b). Thus, the relative magnitude of the 99<sup>th</sup> percentile residual is about 0.001% of the 99<sup>th</sup> percentile tendency term during the peak intensifying stage. Compared to the V tendency, the W tendency exhibits narrower features in the horizontal direction (Fig. 4) with an overall smaller magnitude in every term. The two largest forcings, PGFBUOY and CUV, usually have opposite signs, so their combined effect is on the same order as the ADV and the W tendency term. While the contribution from the upper-layer vertical velocity damping is not shown in Fig. 4 as it is generally small in the low layers, it is included as part of the rhs ( $P_W$ ) of Eq. (2) when calculating the residual for the inline budget analysis. The residual in the inline W budget is generally four orders of magnitude smaller than its tendency term. The 99% percentile residual for W budget is about  $2 \times 10^{-10} \text{ ms}^{-2}$ , around 0.0003% of the 99% percentile w tendency during the peak intensifying stage of the convection (not shown).

### 3.2 Post-processed momentum budget analyses

#### 3.2.1 Key features and methodologies

In contrast to extracting terms directly from the model during its integration, most of the studies in which the momentum budget analysis is conducted use the model output files after the completion of the integration. Note that since the sub-output-time-step information are not available between successive outputs, only the large-step forcing terms can be estimated in these post-processed budget analyses. Generally, the neglect of the acoustic/small-step modes is expected to have little impact on the results as the high-frequency modes are often considered meteorologically insignificant. However, it is mentioned in Klemp et al. (2007) and Skamarock et al. (2008) that the WRF small-step integration scheme includes not only the acoustic-wave but also some gravity-wave modes, which may not be insignificant. These gravity-wave modes form during the small-step integration due to the designated terms that are required for acoustic-wave propagation and “Consequently, in this vertical coordinate (i.e., terrain-following hydrostatic pressure coordinate), the terms governing the acoustic and gravity wave modes are intermingled to the extent that it does not appear feasible to evaluate any of the gravity wave terms on the large time steps, even if one desired to do so.” (Klemp et al. 2007).

Most of the studies did not reveal the complete details about how their analysis was done, so we cannot presume their methodologies and the possible errors. However, a few simplifications commonly made in the post-processed budget analyses

Deleted: .

Deleted: (

Deleted: ).

Deleted: .

Deleted: in Fig.

Deleted: (the inline retrieval method is indicated by the black solid line), which

Deleted:  $3 \times 10^{-8}$

Deleted: Meanwhile,

Deleted: value

Deleted: 004

Deleted: on the order of  $10^{-9} \text{ ms}^{-2}$  (Fig. 4).

Deleted: from Eq. (2)

Deleted: 0.003

Deleted: variables

Deleted: -

Deleted: impacts

may introduce errors that result in deviations from the simulated results and thus a significant residual. Below we revisit the relevant features of the WRF model that should be considered and discuss how they might affect the post-processed budget if they are ignored. Then, the results are shown for different post-processed budget analyses with different simplifications (Table 1). The aim herein is to identify these potential errors hidden in the budget calculation and **show** how severely they affect the resulting interpretation.

#### (a) Diagnosed tendency

In a post-processed budget analysis, the tendency term of a given variable is approximated by the difference between the value of this variable at two successive output **times** divided by the output **time** interval. Thus, the accuracy **may be** sensitive to the output **time** interval. The value at the predicted state has a form of

$$\left. \frac{\partial \Phi^{t+\Delta t}}{\partial t} \right|_{\text{diagnosed}} \approx \frac{\Phi^{t+\Delta t} - \Phi^{t+\Delta t - \Delta t_{\text{output}}}}{\Delta t_{\text{output}}}. \quad (8)$$

If the output interval is longer than the model integration time step, the diagnosed tendency would deviate from the model prediction of the instantaneous tendency. To increase the accuracy, the output time interval  $\Delta t_{\text{output}}$  needs to be similar to the integration time step  $\Delta t$ .

#### (b) Spatial discretization on the C staggered grid

For computational efficiency and accuracy, WRF utilizes a C-grid staggering system (Arakawa and Lamb 1977). This staggering system is pertinent to the numerical solution for spatial derivatives. For most of the spatial derivatives other than advection (e.g., the pressure gradient force), the second-order **finite difference** operator is used in the WRF model. For example, the y-derivative of **variable**  $\Phi$  is calculated using the discrete operator:

$$\frac{\partial \Phi}{\partial y}_{i,j,k} = \frac{1}{\Delta y} \left( \Phi_{i,j+\frac{1}{2},k} - \Phi_{i,j-\frac{1}{2},k} \right). \quad (9)$$

The index  $(i, j, k)$  corresponds to a location with  $(x, y, \eta) = (i\Delta x, j\Delta y, k\Delta \eta)$ , where  $\Delta x, \Delta y$  and  $\Delta \eta$  are the grid lengths in the two horizontal and vertical directions, (can be vertically stretched), respectively. The same expression applies for the x- or the  $\eta$ - derivatives. Grid staggering implies that different variables may be located on different grids, i.e., **shifted by a half-grid point from the others as illustrated in Fig. 6**. Depending on what variable the spatial derivatives are intended for, Eq. (9) should be carried out on the corresponding grid, which is not necessarily the same as the  $\Phi$  grid. For example, for the V tendency, all the associated forcing terms involving the spatial derivatives should be performed on the V grid. More specifically, to calculate the PGF term for the V tendency equation, the term  $\frac{\partial p}{\partial y}$  and the term  $\frac{\partial p}{\partial \eta}$  in Eq. (1) should be calculated on the V grid but not the pressure grid (p grid). Applying Eq. (9) for  $\frac{\partial p}{\partial y}$ , the V grid with location indices of  $(i, j - \frac{1}{2}, k)$  and  $(i, j + \frac{1}{2}, k)$  falls exactly on the p grid and hence no interpolation is required (red arrows in Fig. 6a). However, for  $\frac{\partial p}{\partial \eta}$ , the pressures on the V grid with indices of  $(i, j, k - \frac{1}{2})$  and  $(i, j, k + \frac{1}{2})$  must be obtained (red arrows in Fig. 6b) through linear interpolation using their surrounding closest four pressure values, e.g.,

<b>Deleted:</b> is
<b>Moved down [1]:</b> shifted by a half-grid point from the others as illustrated in Fig. 6.
<b>Deleted:</b> in which some variables are arranged on grids that are
<b>Deleted:</b> , e.g., the pressure gradient and the advection.
<b>Deleted:</b> ,
<b>Deleted:</b> centered
<b>Deleted:</b> for finite differencing
<b>Deleted:</b> variable
<b>Deleted:</b> the
<b>Deleted:</b> ,
<b>Deleted:</b> strategy
<b>Deleted:</b> x
<b>Deleted:</b> $\eta$
<b>Deleted:</b> When
<b>Moved (insertion) [1]</b>
<b>Deleted:</b> are staggered,
<b>Deleted:</b> first rule of thumb is that the locations indicated as $(i, j, k)$ , $(i, j + \frac{1}{2}, k)$ and $(i, j - \frac{1}{2}, k)$ shown in
<b>Deleted:</b> on
<b>Deleted:</b> grid
<b>Deleted:</b> "targeted" prognostic variable. That is,
<b>Deleted:</b> to calculate budget analysis
<b>Deleted:</b> rhs
<b>Deleted:</b> estimated
<b>Deleted:</b> -grid. Taking the PGF for V tendency as an example
<b>Deleted:</b> (1), pressure values at locations
<b>Deleted:</b> V-
<b>Deleted:</b> are
<b>Deleted:</b> according to Eq. (9)
<b>Deleted:</b> An interpolation to the target location might be necessary before applying the discrete operator, as in the case for deriving the term $\frac{\partial p}{\partial \eta}$ in Eq. (1). In this case,
<b>Deleted:</b> at locations
<b>Deleted:</b> on the V-grid are calculated by taking a
<b>Deleted:</b> the
<b>Deleted:</b> available
<b>Deleted:</b> from their original grids (Fig. 6b),

$$p_{v-grid(i,j,k-\frac{1}{2})} = \frac{\frac{1}{2}(p_{p-grid(i,j-1,k)} + p_{p-grid(i,j,k)})\frac{\Delta\eta_{k-1}}{2}}{\frac{1}{2}(\Delta\eta_k + \Delta\eta_{k-1})} + \frac{\frac{1}{2}(p_{p-grid(i,j-1,k-1)} + p_{p-grid(i,j,k-1)})\frac{\Delta\eta_k}{2}}{\frac{1}{2}(\Delta\eta_k + \Delta\eta_{k-1})} \quad (10)$$

which is weighted by the irregular (stretched) vertical grid-lengths (Fig. 6b).

If the C-grid staggering is not considered during the post-processing analysis, i.e., all the variables have been interpolated on the universal grids before carrying out the budget calculation, in addition to the potential errors brought on by the interpolation method, the term  $\frac{\partial p}{\partial y}$ , for example, would essentially involve pressure differences over a larger grid interval of

2 $\times\Delta y$  instead of  $\Delta y$ , with larger associated truncation errors.

(c) Advection operators

For advection, higher-order operators for finite differencing are provided as the default WRF setup. Taking the y component of the flux-form advection for V momentum in Eq. (3) as an example, with a fifth-order operator as selected in the present simulation, it is written as:

$$-\frac{\partial(Vv)}{\partial y}_{i,j,k} \approx -\frac{1}{\Delta y} \left( v_{i,j+\frac{1}{2},k} v_{i,j+\frac{1}{2},k}^{5th} - v_{i,j-\frac{1}{2},k} v_{i,j-\frac{1}{2},k}^{5th} \right) \quad (11)$$

where V and v are the mass coupled- and uncoupled-velocities, respectively.

$$v_{i,j-\frac{1}{2},k}^{5th} = v_{i,j-\frac{1}{2},k}^{6th} - \text{sign} \left( v_{i,j-\frac{1}{2},k} \right) \frac{1}{60} \left[ (v_{i,j+2,k} - v_{i,j-3,k}) - 5(v_{i,j+1,k} - v_{i,j-2,k}) + 10(v_{i,j,k} - v_{i,j-1,k}) \right]_z$$

and

$$v_{i,j-\frac{1}{2},k}^{6th} = \frac{1}{60} [37(v_{i,j,k} - v_{i,j-1,k}) - 8(v_{i,j+1,k} + v_{i,j-2,k}) + 1(v_{i,j+2,k} + v_{i,j-3,k})]_z$$

The odd-order advection operators include a spatially centered even-order operator and an upwind diffusion term. A detailed discussion on the advection scheme in the WRF model with different-order operators can be found in Wicker and Skamarock (2002) and Skamarock et al. (2008). Simplifying the advection estimation using an operator with order that differs from the numerical setup would contribute to errors in the ADV estimation.

(d) Forward/backward Euler method

Conceptually, the WRF model can be considered more of a forward scheme, i.e., using the known variables from the current state to calculate the forcing and then advancing the variables forward until reaching the prediction time. However, there are a few implicit components during the integration. For example, as discussed in Sect. 2.1, the large-step forcings are updated using a predictor-corrector method in the second and third RK3 steps. In addition, the W equation is coupled with the geopotential tendency equation and includes a forward-in-time weighting that utilizes predicted states of the geopotential and temperature in solving the W (Eqs. (3.11), (3.12) and (3.19) in Skamarock et al., 2008).

In numerical analysis for solving ordinary differential equations, the (explicit) forward Euler method approximates the change of a system from  $t$  to  $t + \Delta t$  using the current states ( $t$ ) while the (implicit) backward Euler method finds the solution using the predicted states ( $t + \Delta t$ ):

Deleted: in which different weights are applied because of

Deleted: .

Deleted: Eq. (9)

Deleted:  $\Phi_{i,j+1,k}$  and  $\Phi_{i,j-1,k}$

Deleted: for the WRF users

Deleted: .

Deleted: ]

Deleted: ]

Deleted: indicate the neglect of some terms and a resulting source of

Deleted: predicting

$$\frac{\partial \Phi^{t+\Delta t}}{\partial t} \approx F(\Phi^t) \text{ forward Euler method} \quad (12)$$

$$\frac{\partial \Phi^{t+\Delta t}}{\partial t} \approx F(\Phi^{t+\Delta t}) \text{ backward Euler method} \quad (13)$$

Consistent with this concept, the rhs forcing terms of a budget equation can be estimated using two different instantaneous states in analogous ways. However, we emphasize that the post-processed budget analysis does not solve the tendency equation per se but only diagnoses the relationship between the two sides of the equation. Note that for post-processing analyses, the availability of the data depends on the output time interval ( $\Delta t_{\text{output}}$ ), which is often much larger than the integration time step ( $\Delta t$ ). Thus, for the tendency at a given time  $t + \Delta t$ , when applying the forward Euler method to estimate the associated rhs forcings, the “current states” one can use are the most recent prior output at  $t + \Delta t - \Delta t_{\text{output}}$  (see Fig. 7):

$$\frac{\partial \Phi^{t+\Delta t}}{\partial t} \approx F(\Phi^{t+\Delta t - \Delta t_{\text{output}}}) \text{ forward Euler method for post-processing} \quad (14)$$

If  $\Delta t_{\text{output}}$  is the same as  $\Delta t$ , Eq. (14) reverts to Eq. (12). If  $\Delta t_{\text{output}}$  is much larger than  $\Delta t$ , the backward Euler method using predicted states at  $t + \Delta t$  may better estimate the true model forcing terms as they are calculated using variables at a closer time to the real integration window in the model (Fig. 7).

The above two diagnostic methods estimate the forcing terms using instantaneous states. However, as mentioned in Sect. 3.2.1(a), the diagnosed lhs tendency depends on two successive model output times. Thus, an average between forcings diagnosed explicitly and implicitly are often considered. For a post-processed analysis, this translates into estimating the forcings using both predicted states and the most recent prior available current states:

$$\left. \frac{\partial \Phi^{t+\Delta t}}{\partial t} \right|_{\text{diagnosed}} \approx \frac{1}{2} [F(\Phi^{t+\Delta t - \Delta t_{\text{output}}}) + F(\Phi^{t+\Delta t})]. \quad (15)$$

(e) Flux or advective form of equation

While the momentum equations solved in the WRF model are in flux form, their corresponding advective forms can be derived and are often used for post-processed budget analyses for convenience. To derive the advective form, the flux-form V momentum equation (Eq. (1) excluding residual) is first multiplied by a factor of  $\frac{1}{\mu_d}$  and V is rewritten as  $\mu_d \mathbf{v}$ :

$$\underbrace{\frac{1}{\mu_d} \frac{\partial (\mu_d \mathbf{v})}{\partial t}}_{\text{V tendency}} = - \underbrace{\frac{1}{\mu_d} \nabla \cdot (\mu_d \mathbf{v} \mathbf{v})}_{\text{advection ADV}} + \underbrace{\frac{1}{\mu_d} \left[ -\alpha \frac{\partial p}{\partial y} - \frac{\alpha}{\alpha_d} \frac{\partial p}{\partial \eta} \frac{\partial \phi}{\partial y} \right]}_{\text{horizontal pressure gradient force PGF}} - \underbrace{\frac{1}{\mu_d} f U}_{\text{Coriolis COR}} - \underbrace{\frac{1}{\mu_d} \left( \frac{vW}{r_e} \right)}_{\text{curvature CUV}} + \underbrace{\frac{1}{\mu_d} P_V}_{\substack{\text{remaining} \\ \text{(parameterized)} \\ \text{physics}}} \quad (16)$$

Then, by adding the mass continuity equation in WRF (multiplied by a factor of  $\frac{v}{\mu_d}$ ):

$$\frac{v}{\mu_d} \left[ \frac{\partial \mu_d}{\partial t} + \nabla \cdot (\mu_d \mathbf{v}) \right] = 0$$

to the rhs of Eq. (16), we obtain

Deleted: (

Deleted: .)

Deleted: the

$$460 \quad \underbrace{\frac{1}{\mu_d} \frac{\partial(\mu_d \bar{v})}{\partial t}}_{\text{V tendency}} = \underbrace{\frac{v}{\mu_d} \frac{\partial \mu_d}{\partial t}}_{\text{advection ADV}} + \underbrace{\frac{v}{\mu_d} \nabla \cdot (\mu_d \bar{v})}_{\text{ADV}} - \underbrace{\frac{1}{\mu_d} \nabla \cdot (\mu_d \bar{v} v)}_{\text{ADV}} + \underbrace{\frac{1}{\mu_d} \left[ -\alpha \frac{\partial p}{\partial y} - \frac{\alpha}{\alpha_d} \frac{\partial p}{\partial \eta} \frac{\partial \phi}{\partial y} \right]}_{\text{horizontal pressure gradient force PGF}} - \underbrace{\frac{1}{\mu_d} f U}_{\text{Coriolis COR}} - \underbrace{\frac{1}{\mu_d} \left( \frac{vW}{r_e} \right)}_{\text{curvature CUV}} + \underbrace{\frac{1}{\mu_d} P_V}_{\text{remaining (parameterized) physics}} \quad (17)$$

Moving the first term on the rhs of Eq. (17) to the lhs, the second rhs term can be combined with the flux-form advection using the vector identity  $\nabla \cdot (\mu_d \bar{v}) = \mu_d (\nabla \cdot \bar{v}) + \bar{v} \cdot (\nabla \mu_d)$ . Then, the advective form of the horizontal momentum equation is obtained as:

$$465 \quad \underbrace{\frac{\partial v}{\partial t}}_{\text{v tendency in advective form}} = \underbrace{-\bar{v} \cdot \nabla v}_{\text{advection ADV in advective form}} + \underbrace{\frac{1}{\mu_d} \left[ -\alpha \frac{\partial p}{\partial y} - \frac{\alpha}{\alpha_d} \frac{\partial p}{\partial \eta} \frac{\partial \phi}{\partial y} \right]}_{\text{horizontal pressure gradient force PGF}} - \underbrace{\frac{1}{\mu_d} f U}_{\text{Coriolis COR}} - \underbrace{\frac{1}{\mu_d} \left( \frac{vW}{r_e} \right)}_{\text{curvature CUV}} + \underbrace{\frac{1}{\mu_d} P_V}_{\text{remaining (parameterized) physics}} \quad (18)$$

### 3.2.2 Results of horizontal momentum budget

Table 1 summarizes all the post-processed budget analyses tested in this study. In the present section, we first present the results one by one, and then a qualitative inter-comparison among them and the inline retrieval method is discussed. The first post-processed method (POST10min-E) for V budget follows all the approaches in the model as closely as possible using the 10-min output data. The flux-form equation, C staggering grids, and the same orders of advection operators as the experimental setup are used. The diagnosis of the large-step forcing is applied directly on the model outputs on  $\eta$  levels using the explicit/forward Euler method as shown in Eq. (14). The diagnosed forcing terms are compared with their corresponding true values from the inline retrieval (Fig. 8). Errors smaller than, but on the same order of  $10^{-4} \text{ m s}^{-2}$  as the V tendency, are observed in all terms including the diagnosed tendency term. These errors grow in magnitude and areal coverage with the growth of the disturbance. Aside from COR, the absolute errors in the tendency, ADV and PGF can exceed  $6 \times 10^{-4} \text{ m s}^{-2}$ , the former two of which are more than 50% of the magnitude of their true (instantaneous) values locally.

The second post-processed analysis (POST1min-E) is done following the same approach but applied on the 1-min (same as the integration time step for this simulation) output data, and the results show strongly reduced errors in all terms (Fig. 9). The errors that remain are mostly in the PGF term and likely stem from the fact that the small-step modes and the RK3 integration scheme are not considered in the post-processed budget. These inherent errors result in a small residual term with a general order of  $10^{-5} \text{ m s}^{-2}$ , one to two order(s) smaller than the maximum V tendency. In terms of local maxima, the 99<sup>th</sup> percentile magnitude of the residual obtained in POST1min-E gives a relative magnitude of about 7% of the 99<sup>th</sup> percentile v tendency during the peak intensifying stage of the convection at around 15 hours (Figs. 2b and 5). Although reducing the model output interval to be close to the integration time step helps to balance the budget without the need for inline diagnoses, it is computationally expensive especially for large, data-intensive simulations.

Given that computational cost is often a major consideration, we also test whether the implicit/backward Euler method (POST10min-I) can improve the estimation of instantaneous forcing terms relative to the explicit method for the same 10-min

Deleted: is

Deleted: -

Deleted: acoustic

Deleted: However,

Deleted: can reach

Deleted: 30

output data (POST10min-E). POST10min-I follows the same strategy as POST10min-E except that all the rhs terms, following Eq. (13), are diagnosed with the predicted states instead of the previous output states. As depicted in Fig. 10, POST10min-I indeed better captures the true model estimated forcing values as errors in all the rhs forcing terms diminish greatly to an accuracy similar to POST1min-E. However, as these forcings are calculated at a given instant, the imbalance of the budget would remain if the diagnosed tendency term is not calculated instantaneously (the second to the rightmost column in Fig. 10). Therefore, if budget analysis at an instant of time is desired, we recommend adding the tendency calculation within the model as a standard output and diagnosing the forcing terms implicitly, which yields a residual term on the similar order to the one obtained in POST1min-E (the rightmost column in Fig. 10; Fig. 5a).

For the more common situation, the post-processed analyses diagnose rhs terms using two successive outputs over an output time interval, i.e., taking the averages of the explicitly- and implicitly-calculated forcings using Eq. (15) on the 10-min output (POST10min-(E+I)/2). Comparing the averaged rhs forcings with the analogously-diagnosed lhs momentum tendency (Eq. (8)) gives a small residual to a similar accuracy level as POST1min-E and POST10min-I (the rightmost column in Figs. 11 and 5b).

We now investigate the impact of other common simplifications on top of the reference experiment, POST10min-(E+I)/2. The first such simplification is to approximate the flux-form advection term using the second order operator (Eq. (9)) for both vertical and horizontal components (POST2oadv-(E+I)/2) instead of the third and fifth order operators as used in the model setup. In our simulation, such inconsistency of advection operators introduced errors in the ADV term with a maximum value  $>3 \times 10^{-4} \text{ m s}^{-2}$ , more than 50% of its true magnitude along the slantwise convective band (Fig. 12). Next, we repeated POST10min-(E+I)/2 but the calculation is applied after all the model output variables have been interpolated to the universal/un-staggered grid (pressure grid) (POSTnonstag-(E+I)/2). This is a common way to post-process model output data for plotting purposes. As mentioned earlier, this approach would reduce the accuracy when solving the spatial differential terms and indeed the results indicate significant errors over a large area in both ADV and PGF (Fig. 13). Their combined errors result in widespread residual values  $>3 \times 10^{-5} \text{ m s}^{-2}$  even over the area where the tendency term is smaller than  $1 \times 10^{-4} \text{ m s}^{-2}$  (error is at least of 30% magnitude of the tendency term over a wide area and is reaching 100% over the band head).

Finally, a different format of the V equation, the advective form, is used for post-processed analysis (POSTadvF-(E+I)/2). Mathematically, the flux-form momentum equation can be rewritten in the advective form without making any additional approximation, only with the aid of the conservation law of dry-air mass in the WRF model as shown in Eqs. (16)-(18). However, during the interchange of the expression for the tendency and advection terms, truncation errors may be introduced. We reiterate that the tendency term in the advective form is not equivalent to the one in the flux form divided by  $\mu_d$ , however, calculation suggests that they are approximately equal

$$\frac{1}{\mu_d} \frac{\partial(\mu_d v)}{\partial t} \approx \frac{\partial v}{\partial t}$$

with a maximum error that is on the order of  $10^{-7} \sim 10^{-8} \text{ m s}^{-2}$  (three orders of magnitude smaller than the simulated v tendency) in our study. The summation of the tendency term and advection term in these two forms of the momentum equation

Deleted: remains as

Deleted: .

Deleted: 5

Deleted: where

Deleted: tendency

Deleted: averaged forcings calculated

Deleted: are tested

Deleted: The

Deleted: obtained from this method shows

Deleted: 5

Deleted: to

Deleted: data that

Deleted: same as the one for the

Deleted: variable (p-

Deleted: locally

Deleted: totally

should be mathematically identical, so we would expect to see a small difference in the advection term as in the tendency term. However, we find that the advection term in the advective-form has a strong positive bias compared to that in the flux form (Fig.14). The residual term in the POSTadvF-(E+I)/2 is thus negatively biased over the entire convective band with a magnitude exceeding  $1.2 \times 10^{-4} \text{ m s}^{-2}$  (reaching 100% error near the upper half of the convective band). If the residual is neglected or not shown, authors and/or readers may falsely consider the advection process to be the dominant term governing the evolution of the slantwise updraft.

A quantitative comparison of the 99<sup>th</sup> percentile of the magnitude of the residual term in the domain (excluding the boundaries) among different analysis methods is shown in Fig. 5. The residuals between the instantaneously-diagnosed forcings and the true model tendency term (calculated inline) are shown in Fig. 5a while the ones between the averaged forcings of two consecutive outputs and the diagnosed tendency term are shown in Fig. 5b. The evolution of the 99<sup>th</sup> percentile residual shows generally larger magnitudes when the momentum tendency is larger (Fig. 2b), suggesting that these errors may amplify in stronger convection cases. While the post-processed budget analysis in POST1min-E, POST10min-I and POST10min-(E+I)/2 can achieve a relatively small 99<sup>th</sup> percentile residual (peak at  $\sim 5 \times 10^{-5} \text{ m s}^{-2}$ , or about 7% of the concurrent 99<sup>th</sup> percentile v tendency), the inline budget analysis always gives a much smaller magnitude ( $< 10^{-8} \text{ m s}^{-2}$ , or 0.001% of the tendency, during the entire simulation). Figure 5 also shows that any simplification that is inconsistent with the model solver can severely degrade the accuracy of the post-processed budget analysis. Both POSTnonstag-(E+I)/2 and POSTadvF-(E+I)/2 can lead to a 99<sup>th</sup> percentile of the residual magnitude peaking at around  $4 \times 10^{-4} \text{ m s}^{-2}$  or more, which correspond to  $> 50\%$  of their concurrent 99<sup>th</sup> percentile simulated v tendency, respectively. Generally, a higher relative magnitude of residual to v tendency is reached if the maximum instead of the 99<sup>th</sup> percentile is examined (despite larger fluctuation with time). We also examined the 95<sup>th</sup> percentile of the residual magnitude and obtained qualitatively similar results although the relative magnitudes of such chosen residuals among the three post-processing methods with simplifications (POST2oadv-(E+I)/2, POSTnonstag-(E+I)/2 and POSTadvF-(E+I)/2) vary due to their different error distributions.

### 3.2.3 Results of vertical momentum budget

For the W equation, the closure of the post-processed budget appears not practicable even when the output time interval is reduced to the integration time step (Fig. 15). One partial reason is that the spatially noisy small-step modes, neglected in the offline budget analysis, are surprisingly large with a general order of  $10^{-4} \text{ ms}^{-2}$  over the growing band, which is one order of magnitude larger than the W tendency (see the blue and red contours overlapped on the residual subplots in Fig. 4). These high-frequency modes not only include vertically propagating sound waves but also some gravity wave modes (Klemp et al. 2007). Furthermore, as indicated in Eq. (6) and mentioned in Section 3.1, the W equation solved in the WRF model is implicit, coupled with geopotential tendency equation and includes a forward-in-time averaging operator that is applied on the small-step modes:

$$(\overline{ACOUS})^{\tau} = \frac{1+\beta}{2} (ACOUS)^{\tau+\Delta\tau} + \frac{1-\beta}{2} (ACOUS)^{\tau}$$

Deleted: as  
Deleted: the one

Deleted: 99%

Deleted: values

Deleted: (~2  
Deleted:  $10^{-4}$   
Deleted: <30  
Deleted: , at the peak intensifying stage  
Deleted: value  
Deleted:  $10^{-7}$   
Deleted: <  
Deleted: 004  
Deleted: Any other  
Deleted: impair  
Deleted: term larger than  $10^{-3} \text{ m s}^{-2}$ ,  
Deleted:  $2.2 \times 10^{-3}$   
Deleted: and  $5 \times 10^{-3} \text{ m s}^{-2}$ ,  
Deleted: 300% and >800  
Deleted: -

Deleted: . This  
Deleted: likely because a large portion of model simulated PGFBUOY comes from  
Deleted: implicitly-solved acoustic  
Deleted: which include vertically propagating sound waves and buoyancy oscillations, as shown  
Deleted: our inline  
Deleted: retrieval (Fig. 4). These acoustic modes are spatially noisy over the growing band  
Deleted: ,  
Deleted: 4).

605 where  $\beta$  is a user-specified parameter and  $\Delta\tau$  indicates the small time-step in the acoustic scheme. This means that the small-step modes at a current small-step,  $(\overline{ACOU})^\tau$ , is calculated using information (e.g., geopotential, potential temperature and density) at the forecast time  $\tau + \Delta\tau$  (see Eqs. (3.11) and (3.12) in Skamarock et al. (2008)). All these components are not feasible for an offline budget calculation.

610 The application of POST1min-E for the W tendency shows that this method accurately estimates most of the processes, but large errors  $>2 \times 10^{-3} \text{ ms}^{-2}$  remain in the PGFBUOY term resulting in a widespread residual that reaches the same magnitude of the peak W tendency term (Fig.15). The fact that these errors exceed the small-step modes (contributing to PGFBUOY) suggests that such imbalance does not solely come from the neglect of the small-step modes. A close comparison of the post-processed and the inline PGFBUOY shows that our estimation is close to the inline value to an accuracy of at least three significant figures at the first RK3 step before the acoustic contribution is considered (not shown). However, this large-step forcing term adjusts rapidly, sometime even with a sign change, from step to step within the RK3 integration. Although 615 it is feasible to estimate  $F(\Phi^t)$  via post-processing, it is however impossible to retrieve  $F(\Phi^{**})$  in Eq. (4), leading to the poor estimation of vertical pressure gradient and buoyancy force in the W budget. This result also suggests that the budget closure for vertical velocity is difficult by nature due to its rapid variation in small scales.

#### 4 Tests on different cases or with different horizontal resolutions

620 The growth of the residual as the convection intensifies (Fig. 5) motivates a test on a different case with stronger momentum tendencies. A WRF idealized 2-D squall-line test case (em\_squall2d\_y; Skamarock et al., 2008) is selected with a horizontal resolution of 250 m and 3-second integration time step, and the simulation is integrated for 1 hour. A subgrid turbulence scheme based on the prognostic turbulent kinetic energy equation is activated (Skamarock et al., 2008, chapter 4.2.4). The simulated v tendency in this case is two orders of magnitude stronger than the one in the slantwise convection case. The inline retrieval budget tool works well with 99<sup>th</sup> percentile residuals generally two orders smaller than the tendency terms in the domain during this simulation. However, as compared to the slantwise convection case, this case features a larger relative magnitude of 99<sup>th</sup> percentile residual to the 99<sup>th</sup> percentile tendency term of about 0.1%. Furthermore, the post-processed budget analysis applied on the output data with an output interval the same as the integration time step (analogous to POST1min-E but in this case, it is termed POST3sec-E; Fig. 16), with no simplification made, does not work as well as in the 630 slantwise convection case. POST3sec-E shows that the largest error appears in the PGF term with a magnitude of 50% of its true value at a given instant. The error in diffusion only accounts for about 10% of the error at the same time. One possible reason is that unlike the case of slantwise convection where the PGF exhibits rather horizontally uniform structure with almost the same sign (Fig. 3), the PGF term in this case has a more complex spatial structure with several sign changes over a horizontal distance of 10-15 km. Thus, large errors appear at the edge of these positive/negative patches where the sign changes. Despite the small spatial scales of these errors, the large error magnitude would render accurate interpretation of the physical process difficult based on such post-processed budget analysis. This result suggests that the post-processed budgets, even when done with care, do not always work well, and that the associated residual/errors might be sensitive to the intensity

Deleted: acoustic component of

Deleted: acoustic

Deleted: diffusion

Deleted: a

Deleted: (and a locally peak residual of <0.005 % of the peak tendency term) during this simulation. However

Deleted: While the activated diffusion process is usually difficult to estimate via post-processing and so would be expected to result in some errors, the impact of subgrid turbulence is relatively small at such fine grid spacing (e.g., Bryan et al., 2003). Moreover,

of the simulated system, the spatial/temporal resolution, and the nature of the physical processes governing the different systems.

While an increase in spatial resolution often requires a shorter integration time step for numerical stability and may result in stronger simulated convection, it is almost impossible to separate all these factors. We can, however, conduct the same slantwise convection simulation with a higher resolution of 2 km (and a shorter integration time step of 10 seconds) to exclude the effect of different physical processes in different systems and discuss the changes in the accuracy of the budget analysis when spatial resolution is increased from 10 km. As shown in Fig. 2b, in the 2-km simulation the maximum of the simulated 99<sup>th</sup> percentile v tendency is  $1.2 \times 10^{-3} \text{ ms}^{-2}$ , almost twice the magnitude in the 10-km run. The magnitude of the residual from the inline budget analysis also becomes larger with the 99<sup>th</sup> percentile value almost one order larger than that in the 10-km simulation (Fig. 5). However, its relative magnitude is still small and amounts to about 0.005% of the tendency in the 2-km case. For the post-processed budget analysis applied on the 2-km simulation, the 99<sup>th</sup> percentile residual with the instantaneous calculation of POST10min-I-2km appears only slightly larger yet sometimes smaller than those in its 10-km case (Fig. 5a). For the method using two model outputs for both diagnosed tendency and forcing terms, the peak 99<sup>th</sup> percentile residual in POST10min-(E+I)/2-2km is about four times larger than that in its 10-km counterpart (POST10min-(E+I)/2). This is likely due to the larger deviation caused by the longer diagnosed window (10 minutes) with respect to the integration time step (10 seconds) in the 2-km case. In addition, it appears that the simulated fields adjust more rapidly with more complex structures on smaller scales in the 2-km simulation as compared to the 10-km simulation (not shown). If the same analysis is performed using the 1-min output (POST1min-(E+I)/2-2km) as opposed to the 10-min output, the residual can be greatly reduced to be similar to that obtained in POST10min-(E+I)/2 (Fig. 5b).

The results presented above suggest that the relative magnitude of errors in budget analysis vary with different systems/cases. Furthermore, while the absolute errors in the inline momentum budget analyses indeed increase with increasing horizontal resolution, the relative magnitude with respect to the simulated tendency does not increase substantially. The accuracy of the post-processed budget analysis using the averages of two consecutive model outputs is highly dependent on the ratio of the output interval and the integration time step. A ratio of 10 as used in the POST10min-(E+I)/2 results in an acceptable accuracy (99<sup>th</sup> percentile residual of about 7% of the tendency) while a higher-value of 6 is required for high-resolution simulations (e.g., the 2-km case) to reach a similar accuracy. For cases with a more complex physical process like the squall line test case, the inline budget retrieval appears necessary for adequate budget closure.

## 5 Discussion and summary

Budget analysis is a commonly-employed tool in numerical studies to understand the underlying mechanisms for certain simulated features of interest. However, many studies still have difficulties in achieving a balanced/closed budget especially when a full physics model is used and when the budget is calculated instantaneously over a local area. Aside from the complexity of various (some implicit) parameterization schemes, the main challenge in closing the budget in a full-physics involves the analysis of post-processed data using algorithms that are inconsistent with the model solver. In this study, an

Deleted: value

Deleted: 02

Deleted: in

Deleted: indicates large fluctuation in the 99<sup>th</sup> percentile residual with time (Fig. 5a). While the low values remain similarly small as

Deleted: , the peak values can be two to six times larger.

Deleted: ten

Deleted: only two time larger than the residual

Deleted: 5

Deleted: both

Deleted: and post-processed

Deleted: although

Deleted: for the inline budget analysis

Deleted: Our results suggest that this

Deleted: should be at most

Deleted: (10-km case) and should be even smaller

Deleted: 6 for

Deleted: ).

Deleted: interests

Deleted: to the authors' knowledge

inline momentum budget retrieval tool is developed for the WRF model, and its advantages for momentum budget analysis are demonstrated. The 99<sup>th</sup> percentile residual obtained from this inline retrieval is always smaller than or about 0.1% of the actual tendency term in all the tested cases, which include idealized, 2D simulations of slantwise convection and squall lines. Taking the results from the inline retrieval as “truth”, we investigate the potential errors in each term and the resultant residual for post-processed budget analyses under different assumptions.

705 The comparison among different post-processed diagnoses is focused on the horizontal momentum (V) budget. The reason is that post-processed vertical momentum (W) budget analysis fails to produce reasonably accurate results due to the noisy vertical pressure gradient and buoyancy forces that are tied closely to the small-time-step modes and the implicit scheme used for the vertical momentum integration. Thus, inline retrieval is necessary for an accurate W budget analysis. The errors in the post-processed V budget arise from both the left-hand-side tendency term and the right-hand-side (rhs) forcing terms. To improve the accuracy of the diagnosed momentum tendency estimation, one can reduce the output interval to the model integration time step, which incurs a large computational cost and consumes a large amount of disk space. An alternative and cheaper solution is to add the tendency calculation within the model as a standard output. Our test case of slantwise convection shows that the diagnosed tendency using two successive model outputs with a 10-min interval to approximate the instantaneous true tendency (with an integration time step of 1 minute) could create an error exceeding 50% which greatly limits the effectiveness of such a budget for physical interpretation.

715 For the rhs forcing terms in the V equation, errors can be limited if the post-diagnosis is done with care using the same form of the model equation, the same spatial discretization, the same order of the advection operators, and performing the calculation on the original (e.g., C-staggering and vertically stretched) model grids. However, these steps are necessary but not necessarily sufficient for the closure of the budget, as the forcing term diagnosis also largely depends on the selected input states. If the budget at an instant of time is desired, the explicit/forward Euler method using the previous states might result in large and widespread errors in the advection and horizontal pressure gradient terms (local peak errors are about 50% and 25% of their true values in our simulation, POST10min-E) unless the output interval is reduced to the integration time step. In the latter case (POST1min-E), an error < 5% for each individual term and a residual generally one to two order(s) smaller than the maximum tendency can be achieved (the 99<sup>th</sup> percentile residual is about 7% of the 99<sup>th</sup> percentile v tendency). An alternative way to reach a similar level of accuracy for instantaneous fields without compromising the computational cost is to diagnose the rhs forcings using the implicit/backward Euler method (POST1min-I). This method diagnoses the forcings using the predicted states and thus can better capture the true model forcings by using inputs at a closer time to the model integration window.

720 725 Instead of performing the calculation using model output at one given instant, a more general post-processed budget analysis can use two successive model outputs (POST10min-(E+I)/2). This method seems to work well with the 99<sup>th</sup> percentile residual being about 7% of the 99<sup>th</sup> percentile v tendency in our 10-km case with 10-min output intervals. However, the accuracy of this method varies among the test cases and is sensitive to the ratio of the output interval to the integration time

Deleted: the

Deleted: 02

Deleted: acoustic

Deleted: diagnose

Deleted: .

Deleted: %.

Deleted: the above

Deleted: may

Deleted: be

Deleted:

Deleted: although locally

Deleted: reaches to almost 30

Deleted: instantaneous

Deleted: a

Deleted: term generally one to two order(s) smaller than the maximum

750 step. Among the tests conducted in this study, an upper limit of 10 for this ratio is suggested, and it should be even smaller for high-resolution simulations of high-amplitude weather systems, as rapid adjustments occur on the small scales.

Three other common assumptions in post-processing analysis are made on top of the POST10min-(E+I)/2 to examine their potential impacts on the accuracy of the horizontal momentum budget analysis. First, utilizing an advection operator with a lower order than the one used in the model setup ~~degrades~~ the accuracy of the advection term with up to 50% error over the area where the advection is the strongest (POST20adv-(E+I)/2). Second, the neglect of the staggering grids would negatively impact the estimation of all the spatial differential terms, leading to a widespread residual of at least 30% of the local tendency (POSTnonstag-I). Last, when the advective form of the momentum equation is used for post-diagnosis rather than the flux form, although it is mathematically equivalent to the flux form solved in the model solver, a strong negatively biased residual results (POSTadvF-I). Both POSTnonstag-I and POSTadvF-I gives a peak 99<sup>th</sup> percentile residual of about >50% of the concurrent 99<sup>th</sup> percentile of the v tendency. All the above errors do not just appear randomly; rather, they are spread over the area where the dynamics are the most active, thus undermining the physical interpretation of the dynamics of the simulated system. We thus emphasize the importance of revealing the magnitude of the residual (relative to the tendency term) in publications on budget analysis, to enable readers to gauge the validity of the results.

While the post-processed V budget analysis can reach an acceptable accuracy in some cases, the resultant residual may vary from case to case even when the same analysis method is adopted. Our test of an idealized squall line case with strong momentum tendencies shows that the application of the post-processed budget analysis method without any simplification using the 3-second output data nevertheless results in large relative error magnitude (~50%) in the horizontal pressure gradient force, with very small-scale error structures.

In summary, different assumptions/simplifications made in a post-processed budget analysis may severely impact the estimation of each forcing term and result in a large imbalance of the budget. Based on our experiments, we conclude that the inline retrieval method like that developed herein is the most reliable one for budget analysis in numerical studies. While the budget analyses shown in this study are only for V and W momentum under the 2D idealized configurations, this newly developed budget tool also retrieves budget terms for U momentum and potential temperature. It can be applied to 3D idealized and real cases as the map projection is also considered (i.e., following the original governing equations as shown in Skamarock et al.'s (2008) Eqs. (2.23)-(2.25) with map factors, which are equal to 1 for an idealized setup on the Cartesian coordinate).

We also stress that in some budget studies where a coordinate transformation is necessary (e.g. from Cartesian to polar), some errors are unavoidable. In such cases, it is best to perform the budget calculation using the inline retrieval method on the model grid and then transform the budget to a new coordinate (e.g., Zhang et al., 2000). Finally, in situations where the inline coding cannot be done, this study also provides general guidance to minimize the error in the budget. Thus, our results are beneficial to budget analyses in numerical studies in general, and not limited to the WRF model.

Code availability

Deleted: impairs

Deleted: Its maximum 99<sup>th</sup> percentile residual is even three times larger than the 99<sup>th</sup> percentile momentum tendency term at the strongest intensifying stage.

Deleted: with

Deleted: value almost eight times

Deleted: term (POSTadvF-I).

Deleted: on

Deleted: residual increases with increasing spatial resolution and the results

Deleted: V

Deleted: of errors

Deleted: this study has shown how

Deleted: and

Deleted: .

The standard version of WRF v3.8.1 is publicly available at  
800 [http://www2.mmm.ucar.edu/wrf/users/download/get\\_sources.html](http://www2.mmm.ucar.edu/wrf/users/download/get_sources.html). The inline budget retrieval tool in the WRF v3.8.1  
described in this study can be found at [https://github.com/ting-chenCHEN/WRFV3.8.1\\_inline\\_budget\\_retrieval](https://github.com/ting-chenCHEN/WRFV3.8.1_inline_budget_retrieval) (the version  
for this study is tagged GMD\_submission1) or <https://zenodo.org/record/3373872>. In this repository, all the files that remain  
unchanged from the defaults are tagged as “Initial commit”. The modified files for the budget retrieval include the  
Registry.EM COMMON within the directory Registry; module diag misc.F, module diagnostic driver.F and  
805 module physics addtenc.F within the directory phys; module after all rk steps.F, module big\_step utilities em.F,  
module em.F, module first rk step par2.F, module small\_step em.F and solve em.F within the directory dyn em.

## Appendix A

To our knowledge, there are at least three other similar inline budget retrieval works that have been done in the WRF  
model:

810 (1) Lehner (2012) applied to v3.2.1:

Lehner (2012) provides a very detailed instruction of how an inline budget retrieval is done for the WRF model.  
The method/code was utilized in Lehner and Whiteman (2014) to study the mechanisms of the thermally driven cross-  
basin circulation. However, the code was never made publicly available. From the document, it appears that Lehner  
(2012)’s general procedure of retrieving the rhs budget terms during the model integration is essentially the same as  
815 our approach, which considers both the large-time-step and the small/acoustic-time-step contributions. Furthermore,  
the individual contribution from different parametrization schemes that are activated in her study was also separately  
retrieved. While the general method appears highly similar to our code, the momentum budget retrieval in Lehner  
(2012) only applies to the horizontal momentum (U and V) whereas our tool includes the budget retrieval for the  
vertical momentum (W) as well.

820 (2) Moisseeva (2014), Moisseeva and Steyn (2014) with v3.4.1:

The code is publicly available. The developed budget retrieval is also for the horizontal momentum equations only.  
The method is simpler than Lehner (2012) as it does not include the acoustic/small-step correction terms. Furthermore,  
while the large-time-step, non-parameterized terms (e.g., pressure gradient terms, advection, Coriolis terms...) are  
individually retrieved, their modified Registry file only outputs one (summarized) term for all the parameterized  
825 physics.

(3) Potter et al. (2018) with v3.8.1:

The code is publicly available. This budget retrieval uses the code adapted from Moisseeva (2014), taking references  
from Lehner (2012), and is applied to the same version of the WRF model as used in this study (v3.8.1). More  
components are added from the version used in Moisseeva (2014), including the potential temperature budget, vertical  
velocity budget, the 6th order diffusion term, the parametrized physics term decomposed to boundary layer and  
830 radiation schemes...etc. A major difference from our retrieval tools exists in that the small-step components are

neglected in Potter et al. (2018). Comparing the budget analysis results using our retrieval tool with those using theirs for the same idealized test case of the 2D squall line, the largest differences appear in terms that involve the small-step contributions (e.g., PGF and PGFBUOY), which result in larger residual terms with Potter et al. (2018)'s retrieval method (not shown). While the relative magnitudes of such residuals to the tendency term still appear small for the horizontal momentum budget, they become larger for the vertical momentum budget. This is consistent with our result that the small-step modes are more important in the W budget equation than in the V budget equation and thus ignoring them results in larger errors.

Furthermore, calculations of the lhs tendency terms, i.e., the actual changes of a simulated field with time, are added as new variables in our tool while the tendency terms used in the above studies are the default variables  $ru\_tend$ ,  $rv\_tend$ ,  $rw\_tend$ , etc, which only represent the summation of all the large-step forcings to their corresponding fields (can be directly outputted via changing the WRF Registry file).

## Appendix B

To construct an initial condition that contains conditional symmetric instability (CSI) but to avoid dry symmetric instability and dry and conditional (gravitational) instability is a highly challenging task (Persson and Warner 1995). Therefore, the initial profile in our test case is decided by a trial-and-error method and follows the following steps:

- (1) We first prescribe a horizontally uniform Brunt-Vaisala frequency,  $N^2 = \frac{g}{\theta_v} \frac{\partial \theta_v}{\partial z}$  with a vertical profile of

$$N^2 = \begin{cases} 1.25 \times 10^{-4} & z < 0.5 \text{ km} \\ 9 \times 10^{-5} \text{ s}^{-2} & \text{for } 5 \text{ km} \leq z < 10.5 \text{ km} \\ 5 \times 10^{-4} & z \geq 13.5 \text{ km} \end{cases} \quad (B1)$$

where  $z$  is the height and there is a linear transition for the layers  $0.5 \text{ km} \leq z < 5 \text{ km}$  and  $10.5 \text{ km} \leq z < 13.5 \text{ km}$  using the specified values beneath and above the layers.

- (2) A constant geostrophic vertical zonal wind shear is given,  $\frac{\partial U_g}{\partial z} = 5.8 \times 10^{-3} \text{ s}^{-1}$ . Thermal wind balance gives

$$\frac{\partial U_g}{\partial z} = -\frac{g}{f \theta_v} \frac{\partial \theta_v}{\partial y} \quad (B2)$$

- (3) Based on (B1) and (B2), we can specify the value of  $\theta_v$  at any point and then derive the  $\theta_v$  for the entire domain. In this case,  $\theta_v(y_0, z_0) = 287.5 \text{ K}$  where  $(y_0, z_0)$  indicates the grid at the surface on the southern boundary.

- (4) The relative humidity (RH) field is constructed by specifying a horizontally uniform background profile ( $RH_{background}$ ) with some enhancement ( $RH_{bubble}$ ) over an elliptical area where the initial perturbation will be later added. The enhanced humidity over a limited area hastens the release of CSI and avoids convection developing near the southern boundary.

$$RH_{background}(z) = \begin{cases} 0.81 & z \leq 5 \text{ km} \\ \min \left[ 0.81, 1 - 0.9 \left( \frac{z - 5}{7.5} \right)^{0.8} \right] & 5 \text{ km} < z < 12.5 \text{ km} \\ 0.1 & z \geq 12.5 \text{ km} \end{cases}$$

Deleted: as discussed in

Deleted: (

Deleted: A1

Deleted: where

Deleted: to

Deleted: them

Deleted: The

Deleted: A2

Deleted: Base

Deleted: A1

Deleted: A2

Deleted: one

Deleted: southernmost

Deleted: inserted. The reasons for

Deleted: are to hasten

Deleted: to avoid

Deleted: from

$$RH_{bubble}(y, z) = RH_{background}(z) \times f_{enhancement}(y, z),$$

where

$$f_{enhancement}(y, z) = \begin{cases} 1.22 & e \leq 1 \\ 1.22 - 0.11(e - 1) & 1 < e \leq 3, \\ 1 & e > 3 \end{cases}$$

where  $e = \left(\frac{y-410}{e_b}\right)^2 + \left(\frac{z-1}{e_a}\right)^2$ ,  $e_b = 100$ ,  $e_a = 3$  and  $y$  and  $z$  are the horizontal distance from the southern boundary and height, respectively, with units of km. The constructed initial profile has a maximum RH of 98.82% over an elliptical area centered at  $y = 410$  km and  $z = 1$  km.

(5) A constant surface pressure is specified,  $P_{sfc} = 1000$  hPa.

(6) We then iteratively solve for the hydrostatically balanced pressure, water vapor mixing ratio, potential temperature, dry and full (moist) air density, and geostrophic zonal wind for the entire domain.

The constructed initial environment contains some CSI, which is identified by the presence of negative saturated geostrophic potential vorticity (Chen et al. 2018). In this test case, CSI only exists over the southern half of the domain and never extends higher than 5 km.

To initiate convection, a 2D bubble of potential temperature and zonal wind perturbations is inserted in the area where RH is maximized and where the saturated geostrophic potential vorticity has a value of about -0.2~-0.1 pvu. The center of the bubble, located at  $y = 400$  km and  $z = 1.5$  km, has a maximum potential temperature perturbation  $\Delta\theta_{max} = 0.5$  K and zonal wind perturbation  $\Delta u_{max} = -6$  ms<sup>-1</sup>. Both perturbation fields decrease to zero with radius, following  $\Delta\theta = \Delta\theta_{max} \cos^2(0.5\pi r)$  and  $\Delta u = \Delta u_{max} \cos^2(0.5\pi r)$  where  $r = \sqrt{R^2 + H^2}$ ,  $R = 50$  km is the horizontal radius and  $H = 1.5$  km is the vertical radius.

#### Author contribution

TC designed and performed the numerical experiments under the supervision of MY and DK. MY proposed the idea of comparing the inline and post-processed budget analyses. TC developed the code of the inline budget retrieval tool in the WRF v3.8.1 model and the post-processed analyses. DK provided useful suggestions to improve the work. TC prepared the manuscript and all co-authors contributed to the writing and editing of the paper.

#### Competing interests

The authors declare that they have no conflict of interest.

#### Acknowledgements

The research reported here has been supported by the Fonds de recherche du Québec – Nature et technologies (FRQNT) doctoral research scholarship and the NSERC/Hydro-Quebec Industrial Research Chair program. We thank Patrick

Deleted: -

Deleted: to

Deleted: 2-D

Deleted: maximum

Deleted: perturbation  $\Delta\theta = 0.5$  K

Deleted: perturbation  $\Delta u = -6$  ms<sup>-1</sup>

Deleted: This perturbation bubble has a maximum width of 100 km and thickness of 3 km, with its center located at  $y = 400$  km and  $z = 1.5$  km.

Deleted: processing

Deleted: processing

## References

- Abarca, S. F. and Montgomery, M. T.: Essential Dynamics of Secondary Eyewall Formation. *J. Atmos. Sci.*, 70, 3216–3230, <https://doi.org/10.1175/JAS-D-12-0318.1>, 2013.
- Andersen, J. A. and Kuang, Z.: Moist Static Energy Budget of MJO-like Disturbances in the Atmosphere of a Zonally Symmetric Aquaplanet. *J. Climate*, 25, 2782–2804, <https://doi.org/10.1175/JCLI-D-11-00168.1>, 2012.
- Arakawa, A.; Lamb, V.R.: Computational design of the basic dynamical processes of the UCLA general circulation model. *Methods in Computational Physics: Advances in Research and Applications*. 17, 173–265, <https://doi:10.1016/B978-0-12-460817-7.50009-4>, 1977.
- Arnault, J., Knoche, R., Wei, J. and Kunstmann, H.: Evaporation tagging and atmospheric water budget analysis with WRF: A regional precipitation recycling study for West Africa, *Water Resour. Res.*, 52, 1544– 1567, <https://doi.org/10.1002/2015WR017704>, 2016.
- Balasubramanian, G. and Yau, M. K.: Baroclinic Instability in a Two-Layer Model with Parameterized Slantwise Convection. *J. Atmos. Sci.*, 51, 971–990, [https://doi.org/10.1175/1520-0469\(1994\)051<0971:BIATL>2.0.CO;2](https://doi.org/10.1175/1520-0469(1994)051<0971:BIATL>2.0.CO;2), 1994
- Bryan, G. H., and Fritsch, J. M.: A benchmark simulation for moist nonhydrostatic numerical models. *Mon. Wea. Rev.*, 130, 2917–2928, [https://doi.org/10.1175/1520-0493\(2002\)130<2917:ABSFMN>2.0.CO;2](https://doi.org/10.1175/1520-0493(2002)130<2917:ABSFMN>2.0.CO;2), 2002.
- Chen, T.-C., Yau, M. K., and Kirshbaum, D. J.: Assessment of Conditional Symmetric Instability from Global Reanalysis Data. *J. Atmos. Sci.*, 75, 2425–2443, <https://doi.org/10.1175/JAS-D-17-0221.1>, 2018.
- Duran, P. and Molinari, J.: Tropopause Evolution in a Rapidly Intensifying Tropical Cyclone: A Static Stability Budget Analysis in an Idealized Axisymmetric Framework. *J. Atmos. Sci.*, 76, 209–229, <https://doi.org/10.1175/JAS-D-18-0097.1>, 2019.
- Gallus, W. A., and Johnson, R. H.: The momentum budget of an intense midlatitude squall line. *J. Atmos. Sci.*, 49, 422–450, [https://doi.org/10.1175/1520-0469\(1992\)049<0422:TMBOAI>2.0.CO;2](https://doi.org/10.1175/1520-0469(1992)049<0422:TMBOAI>2.0.CO;2), 1992.
- Grell, G. A., Dudhia, J., and Stauffer, D.: A description of the fifth-generation Penn State/NCAR Mesoscale Model (MM5). NCAR Tech. Note NCAR/TN-398+STR., 121 pp., <https://doi.org/10.5065/D60Z716B>, 1994.
- Hodur, R. M. and Fein, J. S.: A vorticity budget over the Marshall Islands during the spring and summer months. *Mon. Wea. Rev.*, 105, 1521–1526, [https://doi.org/10.1175/1520-0493\(1977\)105<1521:AVBOTM>2.0.CO;2](https://doi.org/10.1175/1520-0493(1977)105<1521:AVBOTM>2.0.CO;2), 1977.

Moved down [2]: J.

Deleted: Bryan, G. H., Wyngaard,

Moved down [3]: C.,

Deleted: and Fritsch,

Moved down [4]: J.

Deleted: M.: Resolution Requirements for the Simulation of Deep Moist Convection. *Mon. Wea. Rev.*, 131, 2394–2416, [https://doi.org/10.1175/1520-0493\(2003\)131<2394:RRFTSO>2.0.CO;2](https://doi.org/10.1175/1520-0493(2003)131<2394:RRFTSO>2.0.CO;2), 2003. .

- Huang, Y.-H., Wu, C.-C., and Montgomery, M. T.: Concentric eyewall formation in Typhoon Sinlaku (2008). Part III: horizontal momentum budget analyses. *J. Atmos. Sci.*, 75, 3541–3563, <https://doi.org/10.1175/JAS-D-18-0037.1>, 2018
- 960 Kanamitsu, M. and Saha, S.: Systematic tendency error in budget calculations. *Mon. Wea. Rev.*, 124, 1145–1160, [https://doi.org/10.1175/1520-0493\(1996\)124<1145:STEIBC>2.0.CO;2](https://doi.org/10.1175/1520-0493(1996)124<1145:STEIBC>2.0.CO;2), 1996.
- Kiranmayi, L., and Maloney, E. D.: Intraseasonal moist static energy budget in reanalysis data. *J. Geophys. Res.*, 116, D21117, <https://doi.org/10.1029/2011JD016031>, 2011.
- Kirshbaum, D. J., Merlis, T. M., Gyakum, J. R. and McTaggart-Cowan, R.: Sensitivity of idealized moist baroclinic waves to environmental temperature and moisture content. *J. Atmos. Sci.*, 75, 337–360, <https://doi.org/10.1175/JAS-D-17-0188.1>, 2018.
- 965 Klemp, J. B., Skamarock, W. C., and Dudhia, J.: Conservative split-explicit time integration methods for the compressible nonhydrostatic equations. *Mon. Wea. Rev.*, 135, 2897–2913, <https://doi.org/10.1175/MWR3440.1>, 2007.
- Kornegay, F. C. and Vincent, D. G.: Kinetic Energy Budget Analysis During Interaction of Tropical Storm Candy (1968) with an Extratropical Frontal System. *Mon. Wea. Rev.*, 104, 849–859, [https://doi.org/10.1175/1520-0493\(1976\)104<0849:KEBADI>2.0.CO;2](https://doi.org/10.1175/1520-0493(1976)104<0849:KEBADI>2.0.CO;2), 1976.
- 970 Kuo, Y. and Anthes, R. A.: Accuracy of diagnostic heat and moisture budgets using SESAME-79 field data as revealed by observing system simulation experiments. *Mon. Wea. Rev.*, 112, 1465–1481, [https://doi.org/10.1175/1520-0493\(1984\)112<1465:AODHAM>2.0.CO;2](https://doi.org/10.1175/1520-0493(1984)112<1465:AODHAM>2.0.CO;2), 1984.
- 975 Lee, C.-S.: The bulk effects of cumulus momentum transport in tropical cyclones. *J. Atmos. Sci.*, 41, No. 4, 590–603, [https://doi.org/10.1175/1520-0469\(1984\)041<0590:TBEOCM>2.0.CO;2](https://doi.org/10.1175/1520-0469(1984)041<0590:TBEOCM>2.0.CO;2), 1984.
- Lehner, M.: Observations and large-eddy simulations of the thermally driven cross-basin circulation in a small, closed basin. Ph.D. thesis, University of Utah, available at: <https://collections.lib.utah.edu/ark:/87278/s61n8fxw>, 2012.
- 980 [Lehner, M. and Whiteman, D. C.: Physical mechanisms of the thermally driven cross-basin circulation. \*Q. J. Roy. Meteor. Soc.\*, 140: 895–907, <https://doi.org/10.1002/qj.2195>, 2014.](#)
- Lilly, D. K., and Jewett, B. F.: Momentum and kinetic energy budgets of simulated supercell thunderstorms. *J. Atmos. Sci.*, 47, 707–726, [https://doi.org/10.1175/1520-0469\(1990\)047<0707:MAKEBO>2.0.CO;2](https://doi.org/10.1175/1520-0469(1990)047<0707:MAKEBO>2.0.CO;2), 1990.
- Liu, L., Lin, Y.-L. and Chen, S.-H., 2016: Effects of landfall location and approach angle of an idealized tropical cyclone over a long mountain range. *Front. Earth Sci.*, 4, 1–14, <https://doi.org/10.3389/feart.2016.00014>, 2016.
- 985 Markowski, P. M., and Richardson, Y.: *Mesoscale Meteorology in Midlatitudes*, Wiley-Blackwell, 424 pp, <https://doi.org/10.1002/9780470682104>, 2010.
- Moisseeva, N.: Dynamical analysis of sea breeze hodograph rotation in Sardinia. B.Sc. thesis, University of British Columbia, available at: <http://hdl.handle.net/2429/46069>, 2014.
- 990 [Moisseeva, N. and Steyn, D. G.: Dynamical analysis of sea-breeze hodograph rotation in Sardinia. \*Atmos. Chem. Phys.\*, 14, 13471–13481, <https://doi.org/10.5194/acp-14-13471-2014>, 2014.](#)

Deleted: ,

Moved (insertion) [2]

Deleted: ,

- Pielke, R.A., and Coauthors: A comprehensive meteorological modeling system—RAMS. *Meteor. Atmos. Phys.*, 49, 69–91, <https://doi.org/10.1007/BF01025401>, 1992.
- 995 Persson, P. O. G. and Warner, T. T.: The Nonlinear Evolution of Idealized, Unforced, Conditional Symmetric Instability: A Numerical Study. *J. Atmos. Sci.*, 52, 3449–3474, [https://doi.org/10.1175/1520-0469\(1995\)052<3449:TNEOIU>2.0.CO;2](https://doi.org/10.1175/1520-0469(1995)052<3449:TNEOIU>2.0.CO;2), 1995.
- Potter, E. R., Orr, A., Willis, I. C., Bannister, D., and Salerno, F.: Dynamical drivers of the local wind regime in a Himalayan valley. *J. Geophys Res-Atmos.*, 123, 13, 186–13, 202, <https://doi.org/10.1029/2018JD029427>, 2018.
- 1000 Powers, J. G., Klemp, J. B., Skamarock, W. C., Davis, C. A., Dudhia, J., Gill, D. O., Coen, J. L., Gochis, D. J., Ahmadov, R., Peckham, S.E., Grell, G.A., Michalakes, J., Trahan, S., Benjamin, S. G., Alexander, C. R., Dimego, G. J., Wang, W., Schwartz, C.S., Romine, G.S., Liu, Z., Snyder, C., Chen, F., Barlage, M. J., Yu, W., Duda, M.G.: The weather research and forecasting model: Overview, system efforts, and future directions. *Bull. Am. Meteor. Soc.*, 98, pp. 1717–1737, <https://doi.org/10.1175/BAMS-D-15-00308.1>, 2017.
- 005 Rios-Berrios, R., Torn, R. D., and Davis, C.: An ensemble approach to investigate tropical cyclone intensification in sheared environments. Part I: Katia (2011). *J. Atmos. Sci.*, 73, 71–93, <https://doi.org/10.1175/JAS-D-15-0052.1>, 2016.
- Sanders, F., and Emanuel, K. A.: The momentum budget and temporal evolution of a mesoscale convective system. *J. Atmos. Sci.*, 34, 322–330, [https://doi.org/10.1175/1520-0469\(1977\)034<0322:tmbate>2.0.co;2](https://doi.org/10.1175/1520-0469(1977)034<0322:tmbate>2.0.co;2), 1977.
- Satoh, M.: Conservative Scheme for the Compressible Nonhydrostatic Models with the Horizontally Explicit and Vertically Implicit Time Integration Scheme. *Mon. Wea. Rev.*, 130, 1227–1245, [https://doi.org/10.1175/1520-0493\(2002\)130<1227:CSFTCN>2.0.CO;2](https://doi.org/10.1175/1520-0493(2002)130<1227:CSFTCN>2.0.CO;2), 2002.
- 1010 Skamarock, W. C., Klemp, J. B., Dudhia, J., Gill, D. O., Barker, D. M., Duda, M. G., Huang, X.-Y., Wang, W., and Powers, J. G.: A description of the advanced research WRF version 3. NCAR Tech. Note NCAR/TN-475+STR, 113 pp. <https://doi.org/10.5065/D68S4MVH>, 2008.
- 015 Thompson, G., Field, P. R., Rasmussen, R. M., and Hall, W. D.: Explicit forecasts of winter precipitation using an improved bulk microphysics scheme. Part II: implementation of a new snow parameterization. *Mon. Wea. Rev.*, 136, 5095–5115, <https://doi.org/10.1175/2008MWR2387.1>, 2008.
- Trier, S.B., LeMone, M.A., and Skamarock, W.C.: Effect of three-dimensional structure on the stormwide horizontal accelerations and momentum budget of a simulated squall line. *Mon. Wea. Rev.*, 126, 2580–2598, [https://doi.org/10.1175/1520-0493\(1998\)126<2580:EOTDSO>2.0.CO;2](https://doi.org/10.1175/1520-0493(1998)126<2580:EOTDSO>2.0.CO;2), 1998.
- 1020 Undén, P., and Coauthors: HIRLAM-5 scientific documentation. Swed. Meteorol. and Hydrol. Inst., 144 pp., available at: <http://www.hirlam.org/>, 2002.
- Wicker, L.J. and Skamarock, W.C.: Time-splitting methods for elastic models using forward time schemes. *Mon. Wea. Rev.*, 130, 2088–2097, [https://doi.org/10.1175/1520-0493\(2002\)130<2088:TSMFEM>2.0.CO;2](https://doi.org/10.1175/1520-0493(2002)130<2088:TSMFEM>2.0.CO;2), 2002.

Moved (insertion) [3]

Moved (insertion) [4]

- 1025 Xue, M., Droegemeier, K. K., and Wong, V.: The Advanced Regional Prediction System (ARPS)—A multiscale  
nonhydrostatic atmospheric simulation and prediction tool. Part I: Model dynamics and verification. *Meteor. Atmos.*  
*Phys.*, 75, 161–193, <https://doi.org/10.1007/s007030070003>, 2000.
- Xue, M., Droegemeier, K. K., and Wong, V., Shapiro, A., Brewster, K. A., Carr, F. H., Weber, D. B., Liu, Y., and Wang, D.:  
The Advanced Regional Prediction System (ARPS)—A multiscale nonhydrostatic atmospheric simulation and  
1030 prediction tool. Part II: Model physics and applications. *Meteor. Atmos. Phys.*, 76, 143–165,  
<https://doi.org/10.1007/s007030170027>, 2001.
- Zhang, D.-L., Liu, Y. and Yau, M. K.: A multiscale numerical study of Hurricane Andrew (1992). Part III: dynamically induced  
vertical motion. *Mon. Wea. Rev.*, 128, 3772–3788, [https://doi.org/10.1175/1520-0493\(2001\)129<3772:AMNSOH>2.0.CO;2](https://doi.org/10.1175/1520-0493(2001)129<3772:AMNSOH>2.0.CO;2), 2000.

1035

**Table 1. A summary of all different approaches for the post-processed horizontal momentum budget analysis that are applied on the model output after the integration finishes.**

	Form of the equation	Output time interval	Order of (vertical; horizontal) advection operators	Forcing terms diagnosed using the explicit or implicit method	Calculated on C staggering grids
Slantwise convection simulation with a grid length of 10 km and integration time step of 1 min.					
POST10min-E	Flux form	10 mins	3; 5	Explicit	Yes
POST1min-E	Flux form	1 min	3; 5	Explicit	Yes
POST10min-I	Flux form	10 mins	3; 5	Implicit	Yes
POST10min-(E+I)/2	Flux form	10 mins	3; 5	Average of explicit and implicit	Yes
POST2adv-(E+I)/2	Flux form	10 mins	2; 2	Average of explicit and implicit	Yes
POSTnonstag-(E+I)/2	Flux form	10 mins	3; 5	Average of explicit and implicit	No
POSTadvF-(E+I)/2	Advective form	10 mins	3; 5	Average of explicit and implicit	Yes
Slantwise convection simulation with a grid length of 2 km and integration time step of 10 secs.					
POST10min-I-2km	Flux form	10 mins	3; 5	Implicit	Yes
POST10min-(E+I)/2-2km	Flux form	10 mins	3; 5	Average of explicit and implicit	Yes
POST1min-(E+I)/2-2km	Flux form	1 mins	3; 5	Average of explicit and implicit	Yes
Squall line simulation with a grid length of 250 m and integration time step of 3 secs.					
POST3sec-E	Flux form	3 secs	3; 5	Explicit	Yes

## WRF Model Integration from $\Phi^t$ (known) to $\Phi^{t+\Delta t}$

### RK3 time integration scheme:

\*including advection, Coriolis, mixing... and all the parameterized physics

(1) 1<sup>st</sup> RK3 step  $\Rightarrow$  Calculate and store all\* the large-step forcing terms (RHS),  $F(\Phi^t)$

$\Rightarrow$  Acoustic integration (one step, with  $\Delta\tau = \Delta t/3$ )

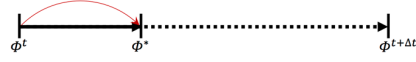
(A) define perturbation variables : for 1<sup>st</sup> RK3,  $\Phi^\tau = \Phi^t, \Phi''^\tau = 0$   
(B) then,  $\Phi''^\tau$  is being advanced through

(a) 1<sup>st</sup> acoustic step

$$\Phi''^{\tau+\Delta\tau} = \Phi''^\tau + F(\Phi^t)\Delta t/3 + [ACOUS(\Phi''^\tau)]$$

$\Rightarrow$  Recover perturbation field to full field

$$\Phi^{\tau+\Delta\tau} = \Phi''^{\tau+\Delta\tau} + \Phi^t = F(\Phi^t)\Delta t/3 + [ACOUS(\Phi''^\tau)] + \Phi^t \equiv \Phi^*$$



(2) 2<sup>nd</sup> RK3 step  $\Rightarrow$  UPDATE and store all the large-step forcing terms (RHS),  $F(\Phi^*)$

$\Rightarrow$  Acoustic integration (2 steps, with  $\Delta\tau = \Delta t/4$ )

(A) define perturbation variables :  $\Phi^\tau = \Phi^*, \Phi''^\tau = \Phi^t - \Phi^*$   
(B) then,  $\Phi''^\tau$  is being advanced through

(a) 1<sup>st</sup> acoustic step

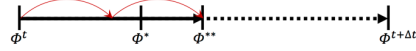
$$\Phi''^{\tau+\Delta\tau} = \Phi''^\tau + F(\Phi^*)\Delta t/4 + [ACOUS(\Phi''^\tau)]$$

(b) 2<sup>nd</sup> acoustic step

$$\Phi''^{\tau+2\Delta\tau} = \Phi''^{\tau+\Delta\tau} + F(\Phi^*)\Delta t/4 + [ACOUS(\Phi''^{\tau+\Delta\tau})]$$

$\Rightarrow$  Recover perturbation field to full field

$$\begin{aligned}\Phi^{\tau+2\Delta\tau} &= \Phi''^{\tau+2\Delta\tau} + \Phi^* \\ &= \Phi''^\tau + F(\Phi^*)\Delta t/2 + [ACOUS \text{ sum}] + \Phi^* \\ &= \Phi^t + F(\Phi^*)\Delta t/2 + [ACOUS \text{ sum}] \equiv \Phi^{**}\end{aligned}$$



(3) 3<sup>rd</sup> RK3 step  $\Rightarrow$  UPDATE and store all the large-step forcing terms (RHS),  $F(\Phi^{**})$

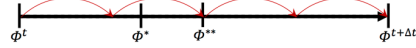
$\Rightarrow$  Acoustic integration (4 steps, with  $\Delta\tau = \Delta t/4$ )

(A), (B)...

(a)-(d) 1<sup>st</sup> -4<sup>th</sup> acoustic step ...

$\Rightarrow$  Recover perturbation field to full field

$$\Phi^{t+\Delta t} = \Phi^t + F(\Phi^{**})\Delta t + [ACOUS \text{ sum}]$$



Compute the contribution from microphysics physics and adjust  $\Phi$

Figure 1: The time integration strategy for advancing a state variable (generalized as  $\Phi$ ) in the WRF model. In this given example, four acoustic steps are specified for one integration time. Adapted from Skamarock et al. (2008).

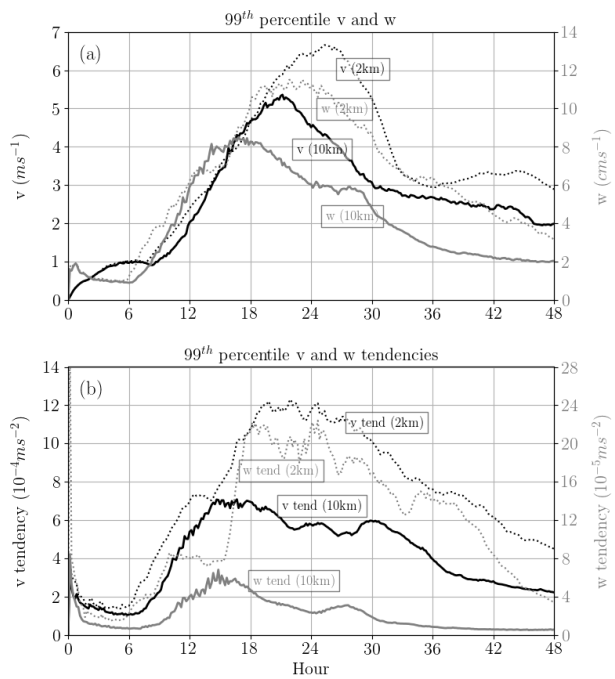
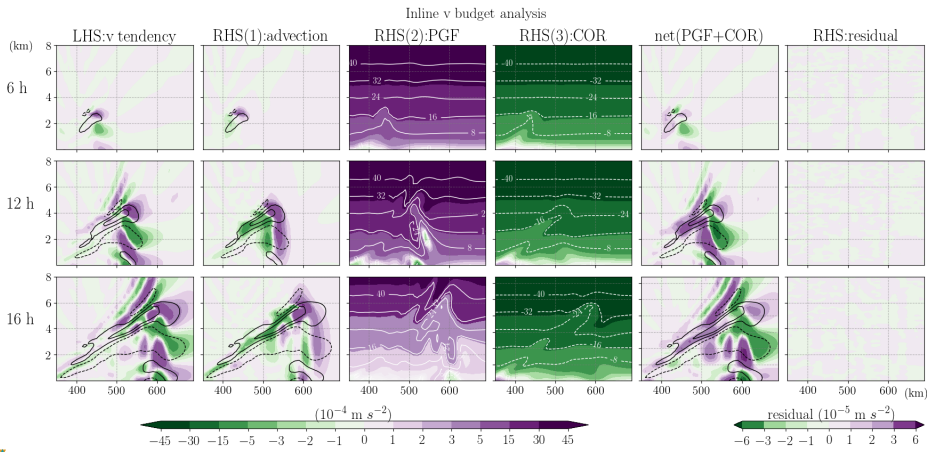


Figure 2. Evolutions of the 99 percentiles of (a) horizontal velocity,  $v$  (black; axis on the left), and vertical velocity,  $w$  (gray; axis on the right) in the simulation of slantwise convection. (b) is same as (a) but for their tendencies (black and gray lines for  $v$  and  $w$  tendencies, respectively). Solid lines are for the 10-km simulation while the dotted ones are for the 2-km case.

050



055

Figure 3. Inline budget analysis of horizontal momentum,  $V$ , with each term extracted directly from the model. In each row, the shading in each subplot from the left to right shows the term of  $V$  tendency, flux-form advection (ADV), horizontal pressure gradient force (PGF), Coriolis force (COR) (white contours indicate the values exceeding the color bar, PGF+COR and residual [Eq. (1);  $P_V$  is zero and the generally small curvature term (CUV) is not shown]. All terms are divided by  $\mu_d$  and thus have units of  $\text{ms}^{-2}$ . The black contours indicate the horizontal velocity  $v$  of 2 and  $6 \text{ ms}^{-1}$  (positive and negative values shown in solid and dashed lines, respectively). Each row from top to bottom illustrates the budget analysis at 6, 12, 16 hour, respectively.

- Deleted:
- Formatted: Font color: Text 1
- Deleted: shaded subplots
- Deleted: show
- Deleted: )
- Deleted: a uniform unit
- Deleted: indicated

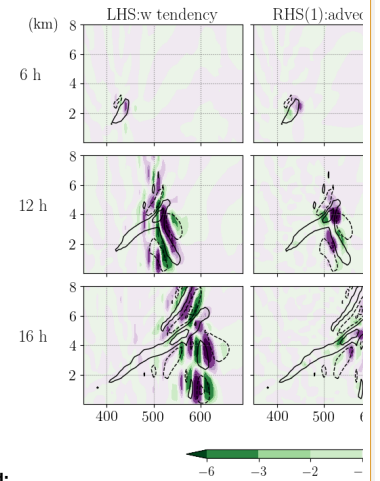
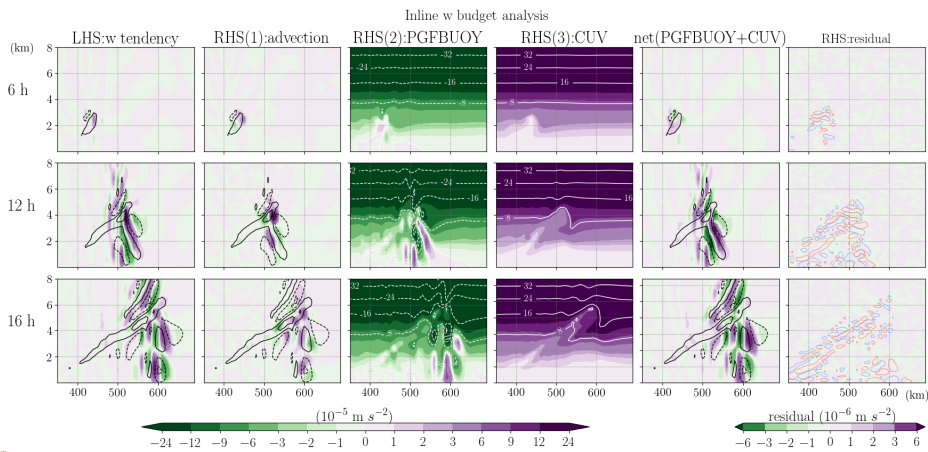


Figure 4. Inline budget analysis of vertical momentum,  $W$ , with each term extracted directly from the model. In each row, the shading in each subplot from the left to right shows the term of  $W$  tendency, advection (ADV), net vertical pressure gradient and buoyancy force (PGFBUOY), curvature (CUV) (white contours indicate the values exceeding the color bar), PGFBUOY+CUV and residual [Eq. (2);  $P_W$  is considered but not shown here]. All terms are divided by  $\mu_4$  and thus have units of  $\text{ms}^{-2}$ . The black contours indicate the vertical velocity  $w$  of 5 and 15  $\text{cms}^{-1}$  (positive and negative values shown in solid and dashed lines, respectively). The red (blue) contours shown in the rightmost column, laid on top of the residual (shading), indicate the small-step components of PGFBUOY with a positive (negative) value of  $3 \times 10^{-4} \text{ms}^{-2}$ . Each row from top to bottom illustrates the budget analysis at 6, 12, 16 hour, respectively.

Deleted:

Formatted: Font color: Text 1

Deleted: shaded subplots

Deleted: show

Deleted: )

Deleted: a uniform unit

Deleted: indicated

Deleted: horizontal

Deleted: acoustic

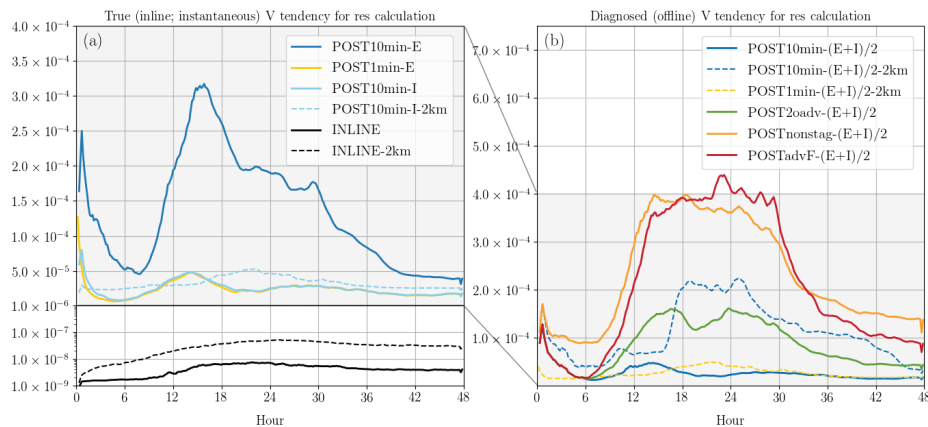
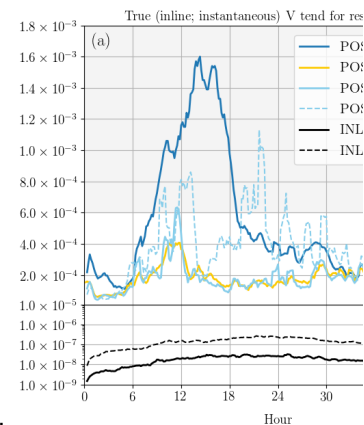


Figure 5. Evolution of the 99th percentile of the residual magnitude ( $\text{ms}^{-2}$ ) of the horizontal momentum V budget analysis. For the residual calculation, (a) uses the true V tendency (derived during the integration of the model) and (b) uses the post-diagnosed V tendency (Eq. (8)) as the lhs term. Different colors indicate different post-processed methods for estimating the rhs forcing terms. The residual obtained from the inline budget retrieval are in black. Solid and dashed lines are for the 10-km run and 2-km run, respectively.



Deleted:

Formatted: Font color: Text 1

Deleted: magnitude of the

Deleted: in

Deleted: )

Deleted: and

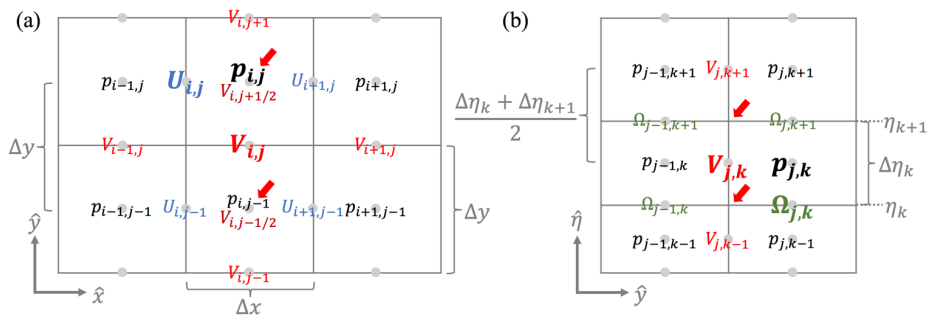
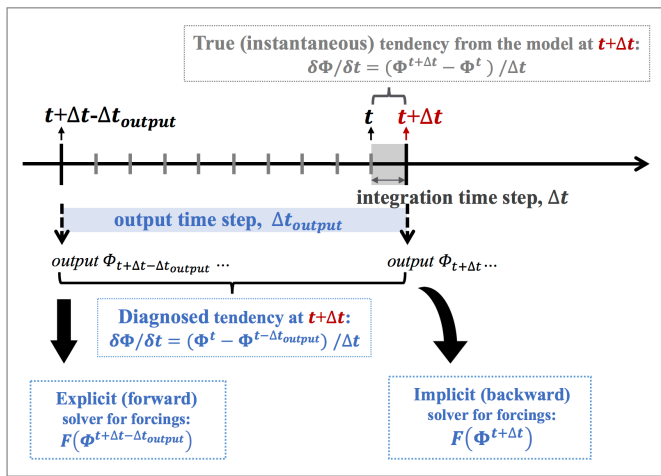
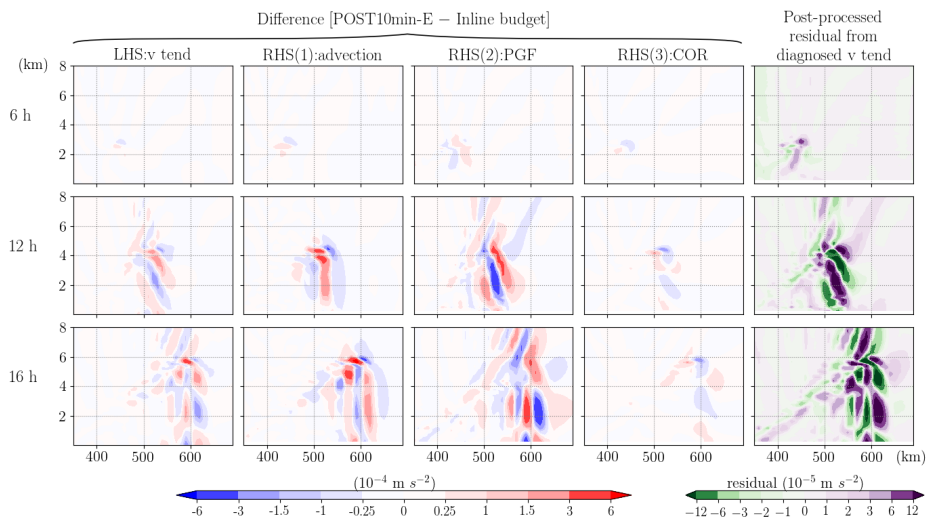


Figure 6. (a) Horizontal and (b) vertical C staggering grids for different variables in the WRF model. Note that variables  $\phi$  and  $W$  are allocated on the same grid as  $\Omega$ ;  $\mu$ ,  $\alpha$  and  $q$ , are on grid same as  $p$ . The red arrows indicate the grids that would be used to calculate the second-order spatial derivative term for the  $V$  momentum at the  $V$  grid  $(i, j, k)$ .

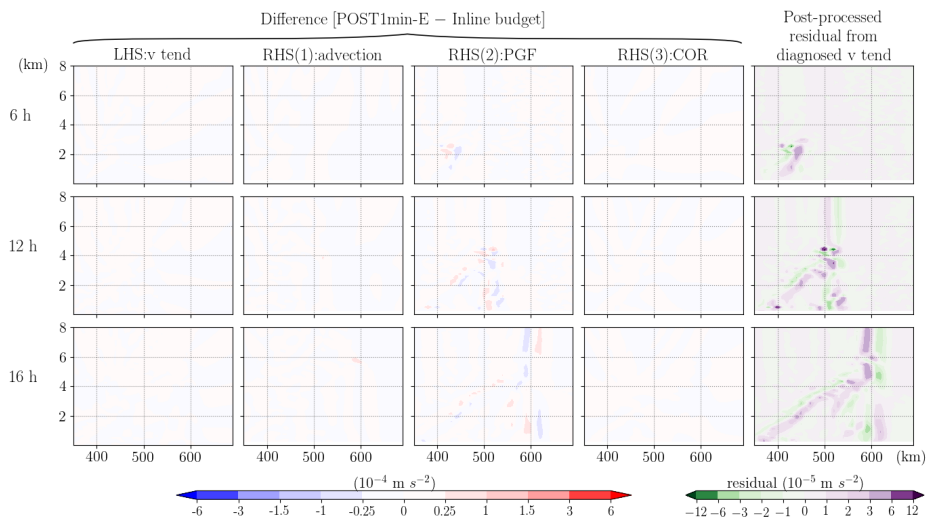
Deleted: -



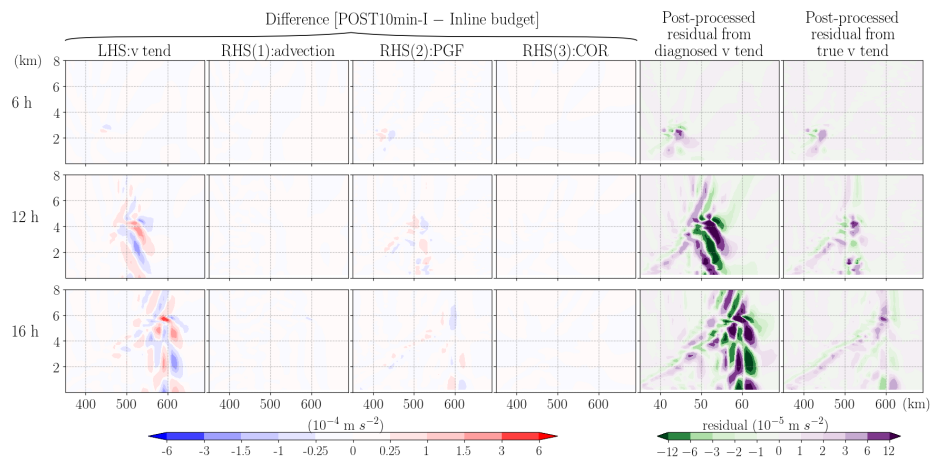
1100 Figure 7. Schematic plot showing the explicit (forward) and implicit (backward) solvers for the rhs forcing terms, as well as the diagnosed and the true (calculated inline during the integration of the model) lhs tendency term defined in this study.



1105 **Figure 8.** The difference between the post-processed (POST10min-E) and inline budget analysis for the horizontal momentum,  $V$ . All terms have been divided by  $\mu_d$  and thus have a uniform unit of  $\text{m s}^{-2}$ . In each row, from left to right indicates the difference for  $V$  tendency, ADV, PGF and COR. The rightmost column indicates the residual term obtained in the post-processed budget analysis. Each row from top to bottom shows the results at 6, 12, and 16 hour, respectively.



1110 **Figure 9.** Same as Fig. 8, but the post-processed budget analysis is applied on the data with an output time interval of 1 minute (POST1min-E).



1115 **Figure 10.** Same as Fig. 8, but the post-processed rhs terms are diagnosed implicitly (POST10min-I) and an extra column is added on the rightmost showing the residual from the true tendency (i.e., the instantaneous value obtained from the model).

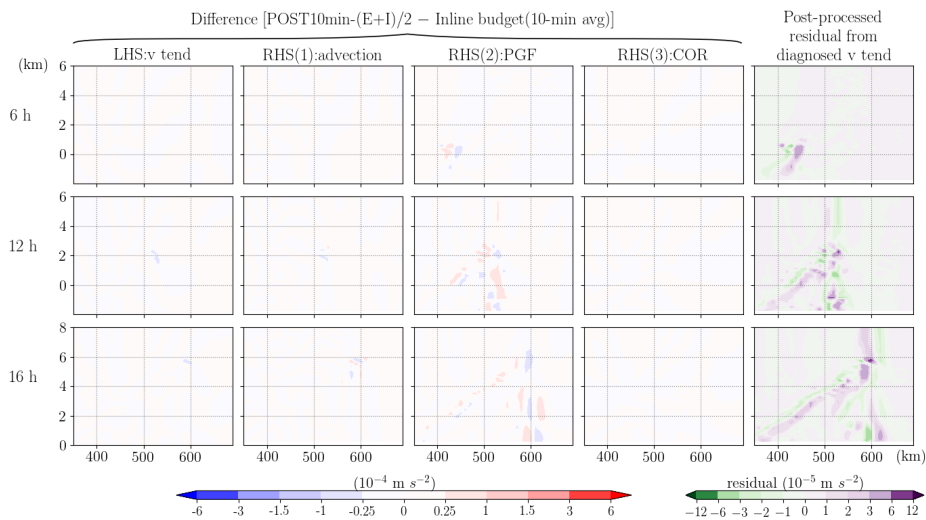


Figure 11. Same as Fig. 8, but the forcing terms diagnosed in the post-processed budget analysis are the average of explicit and implicit methods (POST10min-(E+I)/2). To represent the same time window as the post-processed analysis, the inline budget results used here for the difference calculation are the 10-min averages (corresponding to the output interval) instead of the instantaneous values.

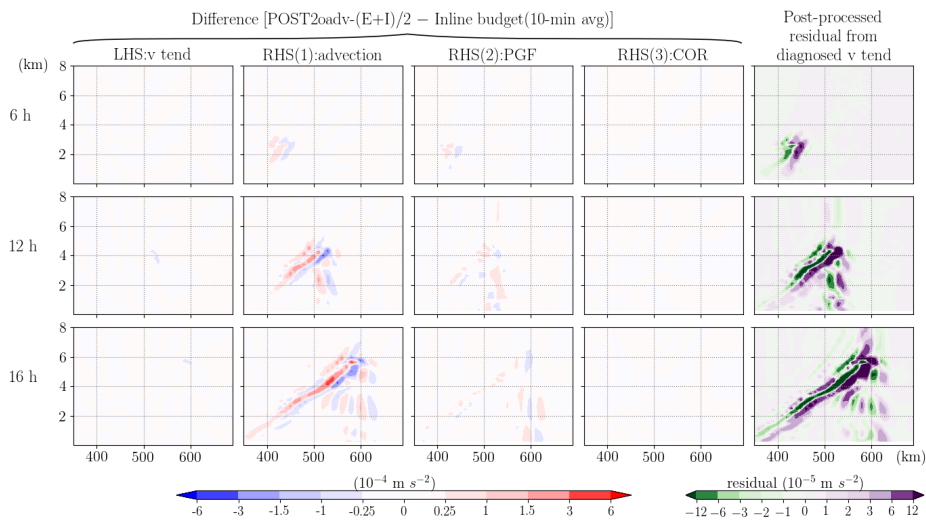


Figure 12. Same as Fig. 11, but the post-processed analysis uses a second order operators for advection calculation ( $\text{POST2oadv}-(E+1)/2$ ).

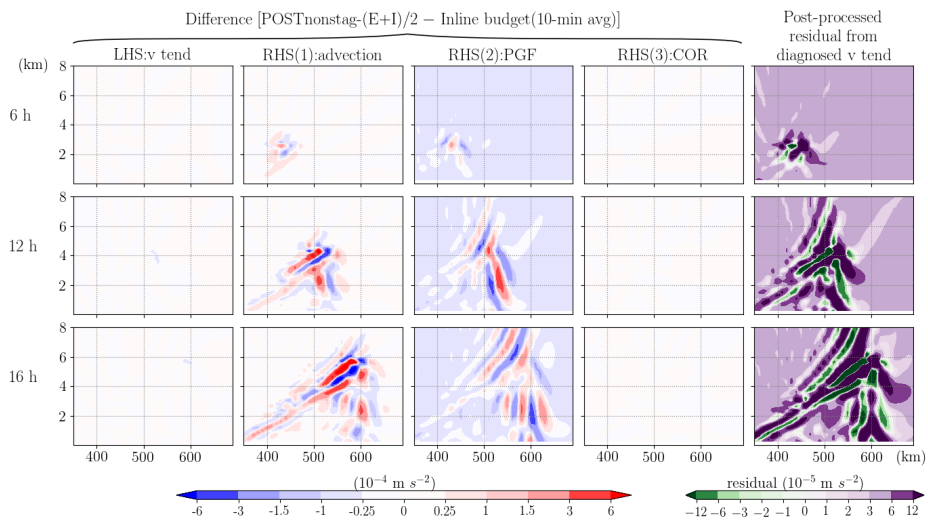
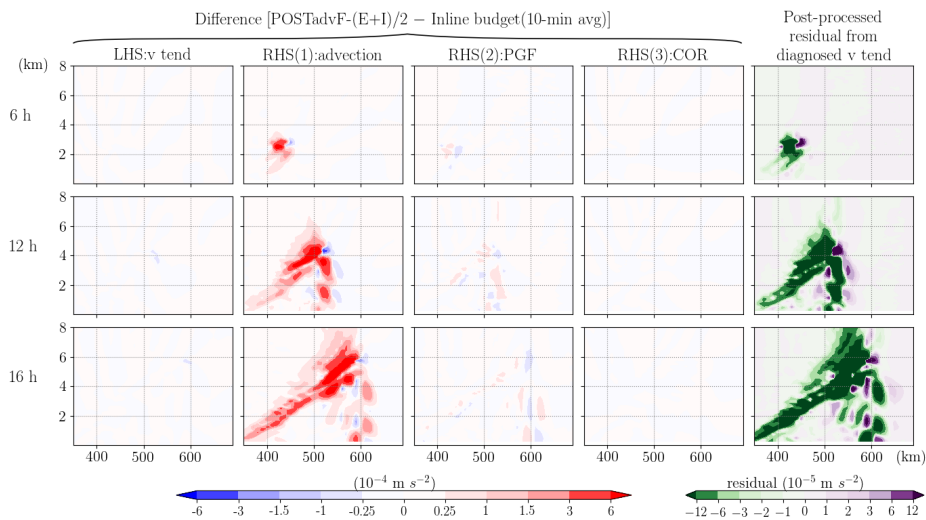


Figure 13. Same as Fig. 11, but for the post-processed analysis does not consider C staggering grids (POSTnonstag-(E+I)/2).



1130 Figure 14. Same as Fig 11, but for the post-processed analysis is applied on the advective-form equation ( $\text{POSTadvF}-(E+I)/2$ ).

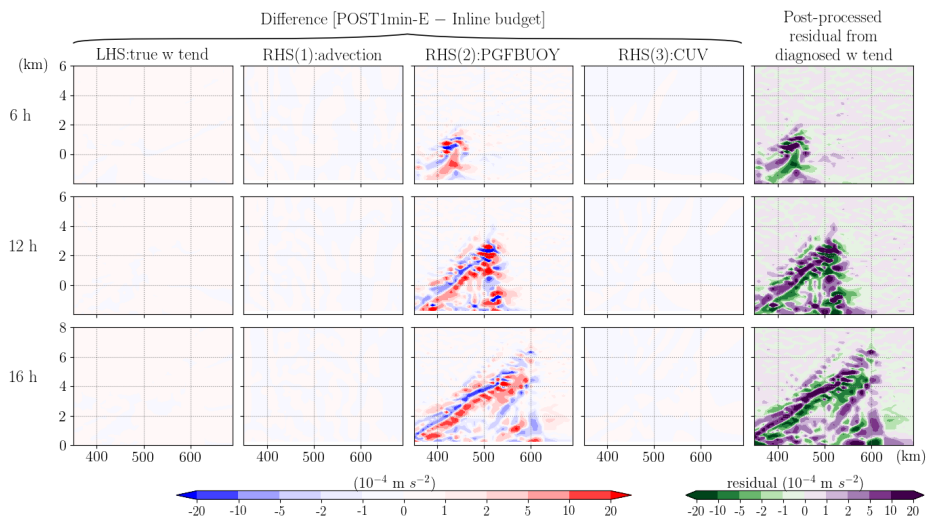


Figure 15. The difference between the post-processed (POST1min-E) and the inline budget analysis for vertical momentum  $W$ . All terms have been divided by  $\mu_d$  and thus have a uniform unit of  $\text{m s}^{-2}$ . In each row, the subplots from left to right indicates the difference of true  $W$  tendency, ADV, PGFBUOY and CUV. The rightmost subplot indicates the residual term obtained in the post-processed budget analysis. Each row from top to bottom shows the results at 6, 12, and 16 hour, respectively.

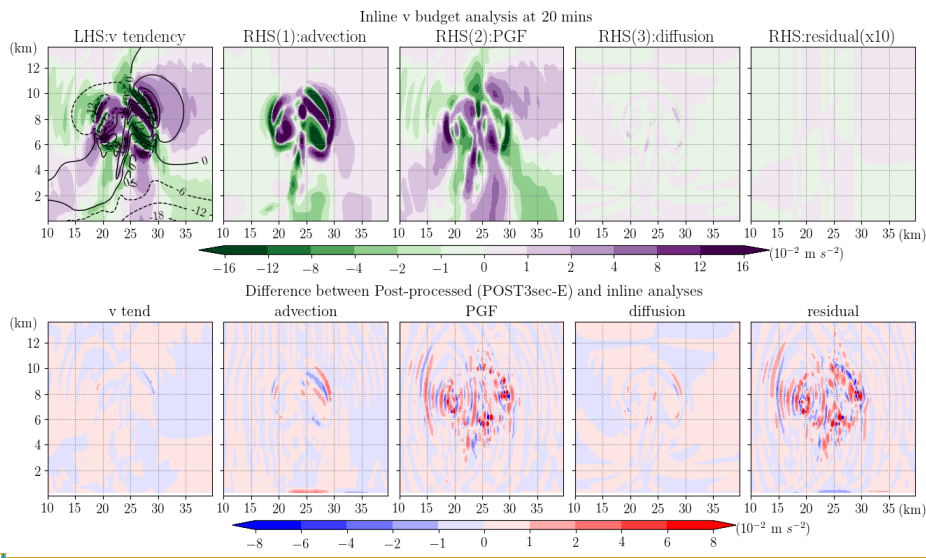


Figure 16. Upper row shows the inline budget analysis of horizontal momentum,  $V$ , for the WRF ideal test case of 2-D squall line at 20 minutes of simulation time. Shading in subplots from left to right represents the term of  $V$  tendency, advection (ADV), horizontal pressure gradient force (PGF), diffusion and residual (multiplied by 10 to emphasize its small magnitude as compared to the other terms). All terms are divided by  $\mu_a$  and thus have units of  $\text{ms}^{-2}$ . The black contours show the velocity,  $v$ , with an interval of  $6 \text{ ms}^{-1}$ . The bottom row shows the difference between the post-processed (POST3sec-E) and the inline budget analysis.

Deleted:

Formatted: Font color: Text 1